Journal of Crystal Growth 312 (2010) 735–749

Contents lists available at ScienceDirect

Journal of Crystal Growth

journal homepage: www.elsevier.com/locate/jcrysgro

Microstructures produced during the epitaxial growth of InGaN alloys

G.B. Stringfellow *

Department of Materials Science, University of Utah, Salt Lake City, UT 84112, USA

ARTICLE INFO

Article history:
Received 10 September 2009
Received in revised form
3 December 2009
Accepted 5 December 2009
Communicated by T.F. Kuech
Available online 28 December 2009

Keywords:
A1. Low dimensional structures
A1. Nanostructures
A1. Phase equilibria
A3. Organometallic vapor phase epitaxy
B1. Nitrides
B3. Light-emitting diodes

ABSTRACT

Effects due to phase separation in InGaN have been identified as having major effects on the performance of devices, in particular light-emitting diodes (LEDs) and injection lasers. However, the complexity of the various materials phenomena that can occur has led to a great deal of recent confusion. Much of this confusion can be eliminated by considering the experimentally measured materials properties in the context of the set of physical phenomena occurring during epitaxial growth, including coupling that exists between the various effects. Spinodal decomposition is expected to produce phase separation due to the miscibility gap in InGaN alloys. However, the actual occurrence of this phenomenon has been disputed due to the complexity of real systems. For example, the region of solid immiscibility for InGaN is strongly dependent on elastic strain. In addition, the strain, itself, affects properties such as the bandgap energy. Complicating the analysis of these phenomena is that the solid composition can be affected by elastic strain due to the well-known thermodynamic phenomenon of "compositional pulling". An additional factor must be considered if the experimentally observed phenomena are to be understood. Thin, lattice mismatched epitaxial layers are coherent with the substrate (or underlying layer). Thus, the actual growth process for the formation of lattice mismatched layers, namely the Stranski–Krastanov (S–K) formation of islands, must be included in any realistic growth model. By considering all the phenomena together, including the coupling between them, it becomes clear that several separate mechanisms exist for phase separation. The focus of this paper is the analysis of the thin (2–3 nm), coherent InGaN layers used in the quantum well structures used for virtually all LEDs and lasers produced by the S–K mechanism. By considering these coupled phenomena together it is possible to arrive at a coherent interpretation of the various materials properties measured using techniques such as high resolution transmission electron microscopy, X-ray diffraction, and optical techniques as well as the device characteristics.

1. Introduction

InGaN and AlInGaN alloys have assumed increasing importance during the last decade. This is because the bandgap of AlInGaN can be tuned over the entire deep UV–visible–near IR range from 0.7 (bandgap of InN) to 6.2 eV (bandgap of AlN). These alloys are essential for the fabrication of blue, green, and white light-emitting diodes (LEDs) [1,2]. However, the performance of yellow and, especially, red LEDs is poor, probably because of materials quality issues. AlInGaN alloys are also important for solar-blind detectors [3] and high power FETs [4]. Because of the wide range of bandgap tunability, they are also currently being investigated for multi-junction solar cells [5]. In principle, all of the bandgaps required for the most efficient combination of solar cells could be obtained using a single alloy system.

On the other hand, these alloys have also proven to be most difficult to understand and control. The basic properties of the alloys are often masked by the large defect density induced by the lack of a native substrate. This typically means that they are grown on sapphire (or SiC) substrates having a dissimilar crystal structure, lattice spacing, and thermal expansion coefficient [1,2]. This results in epitaxial AlInGaN layers having dislocation densities of 10^8–10^{10} cm^{-2}, in addition to stacking faults, twins, and other defects near the sapphire-epilayer interface [6]. GaN and InGaN alloys for device applications have been grown by molecular beam epitaxy (MBE) and hydride vapor phase epitaxy (HVPE) techniques, but are nearly always grown by organometallic vapor phase epitaxy (OMVPE, also called MOCVD) for commercial LEDs and lasers. Typically, a thin GaN or AlN buffer layer is grown first at a low temperature followed by high temperature ($>1000\,^{\circ}C$) growth of a GaN or AlGaN layer, followed by the growth of InGaN at temperatures ranging from 700 to 900 °C [7]. Typical LED structures consist of multiple quantum wells with well thicknesses of 2–3 nm and In contents ranging from 15% (blue) to 20% (green) InN, and even higher for

* Tel.: +1 801 581 8387; fax: +1 801 581 8692.
E-mail address: stringfellow@coe.utah.edu

0022-0248/$ - see front matter © 2009 Elsevier B.V. All rights reserved.
doi:10.1016/j.jcrysgro.2009.12.018

yellow and red LEDs. The performance of these LEDs is stunningly good, considering the density of threading dislocations [8]. In other III/V semiconductor materials systems a dislocation density of 10^8 cm^{-2} would be sufficient to kill the radiative recombination efficiency [9,10]. For LED performance, a number of materials issues turn out to be of critical importance. Issues relating to OMVPE growth, defect generation, and p-type doping, all major materials issues, will not be dealt with here. Instead, this paper will concentrate on issues related to the basic AlInGaN, or more frequently InGaN alloys, including the control of solid composition, factors leading to non-uniform alloy composition, and deviations from an ideal, random distribution of the cation species. OMVPE will be the main growth technique considered, since it is virtually the sole technique used for the commercial production of LED and injection laser devices. However, critical data obtained for materials grown by MBE will also be considered, where appropriate.

The objective of this paper is to examine the growth of these complex materials as a whole in terms of the basic material phenomena occurring during growth in an effort to better understand the phenomena controlling the microstructure, in particular phase separation. A better understanding of these basic phenomena is vital in our search for tools to control the microstructure and, hence, the materials properties and to, literally, allow the design of these alloys in complex structures for specific device applications. The complex issues involved in understanding the microstructure of InGaN epilayers are typically not considered together. Frequently, experimental observations are considered only in terms of a specific, individual phenomenon, which has led to some confusion. The approach taken here will be to review the basic materials phenomena individually and then to consider the coupling between the various phenomena, which makes the analysis of results more complex. This will be followed by a discussion of the salient materials and device properties in terms of the complex growth phenomena. This allows a consistent interpretation of much of the existing data.

2. Materials phenomena affecting the microstructure of InGaN alloys

2.1. Alloy composition

The first materials issue to be considered is the control of alloy composition. In common with all III/V alloys, before the complexities of the microstructure of the AlGaInN alloys were fully appreciated, the sole parameter thought to control materials properties was the alloy composition. For example, the bandgap energy was considered to be a unique function of solid composition. To this day, the bandgap of GaInN alloys is typically represented as a simple function of alloy composition

$$E_g = A + Bx - cx(1-x) \quad (1)$$

where A is the bandgap of GaN (x=0), $A+B$ is the bandgap of InN (x=1), and c is the bowing parameter. For InGaN at room temperature, the values of the three parameters are 3.42, −2.72, and 1.43 [11,12], respectively, all in units of electron volts. This leads to the curved line in Fig. 1 representing the bandgap versus lattice constant for InGaN. The use of Eq. (1) implies that the alloy consists of a random distribution of the Ga and In atoms on the cation sublattice. Unfortunately, this is not the case when the two cations have different covalent radii, as for InGaN. The actual color of an LED with an InGaN active layer is, in fact, a function of the nominal alloy composition, but with additional effects from strain and the microstructure, as discussed in what follows.

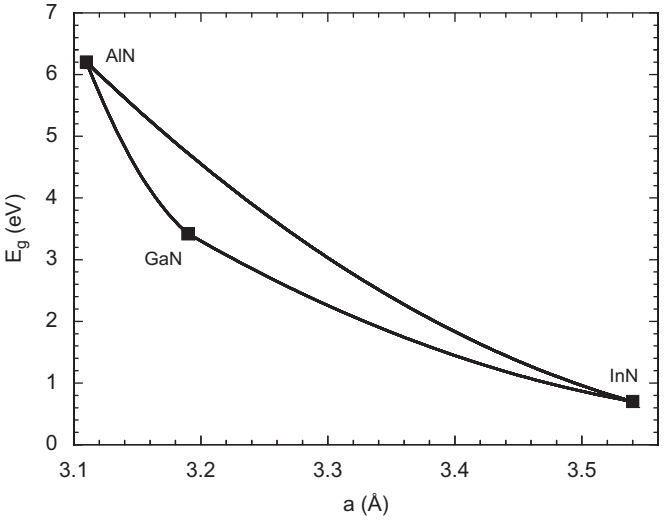

Fig. 1. Bandgap versus lattice constant for AlInGaN alloys (using parameters from Wu et al. [11]).

Before approaching the complex issues of microstructure, we will consider the factors determining solid composition for the hypothetical random alloy, where solid composition does, indeed, uniquely determine the strain-free materials properties, including the bandgap energy. Typically, for alloys with mixing on the cation sublattice grown by OMVPE, the ratio of group III atoms in the solid is approximately equal to the ratio of the group III element precursors in the input vapor phase [13]. Thus, the group III distribution coefficient is typically nearly unity. This is a result of thermodynamic factors, assuming local equilibrium at the solid/vapor interface [13]. The V/III ratio is typically much greater than unity and the enormous supersaturation of the vapor dictates that the group III atoms are used up at the interface. Another way of expressing this is that the vapor pressures of the group III elements at typical OMVPE growth temperatures are extremely small—they are considered to be non-volatile metals. The unity group III distribution coefficient is experimentally observed in a wide range of III/V alloys [13]. The In distribution coefficient for the OMVPE growth of thick InGaN layers is also reported to be unity for growth at 640 °C [14].

As the temperature increases, the basis for this behavior begins to fail. For example, when In is one of the group III elements, and high growth temperatures are used, the In vapor pressure increases and the In distribution coefficient becomes progressively smaller as the temperature increases [1,2,13,15]. At the high temperatures used for the growth of GaN and AlGaN, a significant decrease in In incorporation is observed [16]. Thus, InGaN is grown at substantially lower temperatures, typically from 700 to 900 °C. As we shall see, this has dramatic implications for the determination of the alloy microstructure.

2.2. Strain

After solid composition, strain is the second basic factor affecting materials properties, particularly the bandgap energy, for the ideal random alloy. The relaxed lattice constant of an InGaN layer is virtually always different than that of the underlying layers, whether they are GaN, AlGaN, sapphire, or SiC. The resultant lattice mismatch produces a biaxial strain in the InGaN epitaxial layer

$$\varepsilon = \text{constant}(x - x_o) \quad (2)$$

where x_o is the solid composition giving a lattice match with the underlying layer. For example, in InGaN grown on GaN, x_o=0.

The biaxial strain breaks the cubic symmetry of the lattice and thus acts to alter both the band structure and, in a significant way, the bandgap energy [17]

$$E_g = E_{go} + D\varepsilon \quad (3)$$

where D is the specific deformation potential for the particular direction of biaxial strain and E_{go} is the bandgap energy in the unstrained state. For the direct bandgap III/V semiconductors, the bandgap increases with compressive strain and decreases with tensile strain. The magnitude of the coefficient D is material dependent and is different for the two signs of strain because of the splitting of the valence band degeneracy caused by the biaxial strain [17].

2.3. Lattice pulling

Compounding the effect of strain is that it can directly affect the alloy composition via the phenomenon of "lattice latching" or "composition pulling". This phenomenon was first observed in InGaP layers grown by liquid phase epitaxy (LPE) [18]. It has since been documented in a wide range of materials grown by various techniques [19]. As the system attempts to minimize the free energy of the coherent layer of the solid alloy being grown, strain energy must be considered in addition to the "chemical" energy involved in bond formation. Thus, the solid composition is always perturbed away from the strain-free value in a direction that reduces the lattice mismatch strain energy. In simple terms, the solid composition, x_{epi}, "latches" to the value giving no mismatch with the substrate or underlying layers, x_o, as is observed when the "equilibrium" solid composition, x_{eq}, is near that giving lattice matching [18,20]. Of course, the mismatch does not remain at zero as the difference between the "equilibrium" and "lattice matching" solid compositions becomes large. However, the solid composition is always pulled toward that giving lattice matching, thus "compositional pulling" is the preferred description of this phenomenon. For small values of $x_{eq}-x_o$ the solid composition may be written [20]

$$x_{epi}-x_o = Q(x_{eq}-x_o) \quad (4)$$

where Q is a constant, equal to 0.1 for InGaP grown by LPE on GaAs substrates. Of course, this value will depend on the alloy system.

At higher values of $x_{epi}-x_o$ the relationship shown in Eq. (4) becomes non-linear. When the value of mismatch is large enough, for thick layers ($t > t_c$) dislocations are generated and the layer is no longer coherent. This leads to a value of x_{epi}–x_{eq}=0 [18] for complete strain relaxation. Lattice pulling has been widely observed for InGaN and AlGaN alloys grown by OMVPE [21–25]. As will be seen below, this is a vital factor in obtaining an understanding of the InGaN microstructure.

The two strain effects described above are complex because they are coupled. Strain, which is a function of x, changes the bandgap directly (Eq. (3)) and can also change the solid composition (Eq. (4)), which also changes the bandgap energy (Eq. (1)).

2.4. Ordering

Over the last decade a number of critically important microstructural details, with dramatic impact on materials properties, have come to light for GaInP alloys, in particular, and semiconductor alloys in general. Perhaps the simplest to analyze is atomic-scale ordering. The occurrence of ordering was unanticipated, since the enthalpy of mixing for III/V alloys is always greater than or equal to zero [13,26]. For the widely studied InGaP alloys, used for red and yellow LEDs [27] and multi-junction solar cells [28], the cation distribution is frequently distinctly not random; atomic-scale ordering is observed [13,29]. For (0 0 1) GaInP alloys, the ordering normally produces a {1 1 1} monolayer superlattice, termed Cu–Pt ordering. It is driven by surface thermodynamics due to the surface reconstruction. Other ordered structures have also been observed, depending on the alloy system, the substrate orientation, the growth parameters, and the addition of surfactants during OMVPE growth [29,30]. This is by no means a purely academic phenomenon. Control of Cu–Pt ordering is important for most applications, since it has a major, direct effect on the bandgap energy [29]. Cu–Pt ordering is found to decrease the bandgap energy in GaInP by as much as 160 meV [31], so must be controlled for all devices. Unlike the InGaP alloys, ordering does not appear to be a major factor determining the properties, in particular the bandgap energy, of InGaN, although it may adversely affect LED performance [32]. Thus, it will not be considered further here.

2.5. Phase separation

For the InGaN alloys, a much more critical microstructural phenomenon is the formation of non-uniform alloys due to the occurrence of phase separation (PS) during growth. For the purposes of this paper, PS will be defined as the occurrence of a non-uniform alloy composition in a single InGaN layer. As discussed in Section 3, PS can be caused by a number of different effects. Even though random alloys have some degree of inhomogeneity, they are, by definition, a single phase.

First, we must consider the basic thermodynamics of InGaN alloys. Early valence force field (VFF) calculations of Ho and Stringfellow [33] indicated that the phase diagram for bulk, unstrained, zincblende InGaN has a large region of solid immiscibility at typical InGaN growth temperatures. In Fig. 2, the region within the solid, binodal line defines the alloys that are thermodynamically unstable. Between the binodes the broken line indicates the spinode. For alloys having compositions between the spinodes at a given temperature, there is no energy barrier to PS, i.e., the solid is unstable to any compositional fluctuations. The calculated phase diagram gives a solubility of InN in GaN at 750 °C of $<5\%$, as seen in Fig. 2. The experimental data [34–41] will be discussed below. Later, more detailed VFF and first principles calculations [42] indicate that the equilibrium solubility may even be slightly smaller. This is supported by the work of Karpov et al. [43], where the solubility of wurtzite InN in GaN was calculated to be approximately 4%. The calculations of Gan et al. [44] using density-functional theory appear to be more complete than other first principles calculations. They predict a solubility of wurtzite InN in GaN of only 2%. Even allowing for uncertainties in the calculations, the alloys used for blue and green MQW LEDs (x=0.15 and x=0.20, respectively) are well within the calculated region of solid immiscibility. At equilibrium, these alloys could not be grown. In fact, the non-equilibrium growth of immiscible III/V alloys by OMVPE has been shown to be possible for many alloys [13]. For thick InGaN epilayers, the beginnings of PS by spinodal decomposition occur during OMVPE growth for alloys within the miscibility gap [34–39]. This gives rise to experimentally observed compositional fluctuations within the epitaxial layer. Impressively, the solubility determined from these experiments, agrees quite well with the calculated phase diagram of Ho and Stringfellow, as seen in Fig. 2. Uniform layers were observed for In concentrations less than the solid solubility (binode). For compositions between the spinode and the binode on each side of the phase diagram, the alloys are metastable.

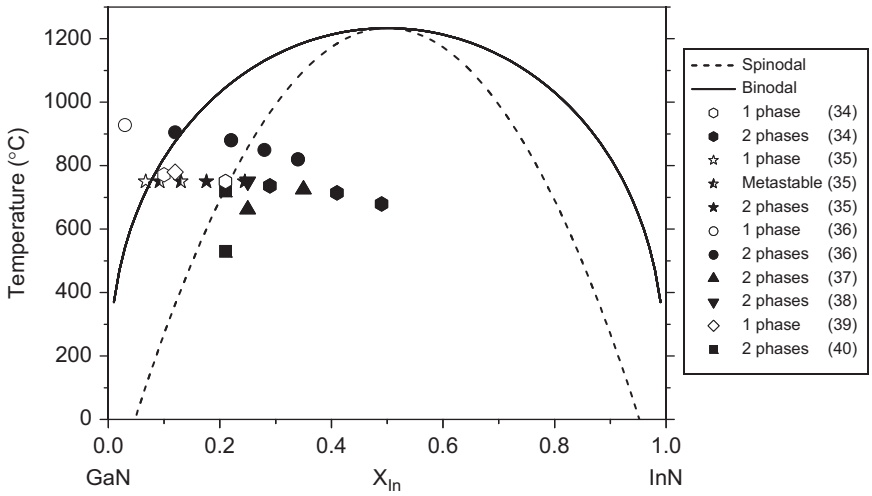

Fig. 2. Calculated binodal (solid) and spinodal (dashed) curves (Ho and Stringfellow [33]) compared to experimental data (Piner et al. [34], Ponce et al. [35], Rao et al. [36], Doppalapudi et al. [37], Kar et al. [38], Faleev et al. [39], and Potin et al. [40]) for GaInN. Open data points=single phase; half-filled data points=metastable; filled data points=2 phase mixtures.

In these regions, an energy barrier must be surmounted for PS to occur. This suggests that PS may occur only near lattice disruptions, such as dislocations and other imperfections. Ponce et al. [35] reported that In-rich regions were formed only at elastically distorted regions of the layers, namely at dislocations for these metastable alloys, although experimental verification was not included. PS in this region is found to vary between the various experimental investigations, as seen in Fig. 2. With larger In concentrations, giving alloys between the spinodes, spontaneous PS was observed throughout the layer in all experimental studies, as indicated in Fig. 2.

In light of the complexities due to elastic strain effects the good agreement between the experimental results and the phase diagram calculated ignoring strain effects, shown in Fig. 2, is perhaps surprising. It suggests that the elastic strain, for the thick layers in all of these experimental studies, is reduced significantly during OMVPE growth. This may be due to the generation of misfit dislocations. Indeed, the results of Ponce et al. [35] show the lattice parameters for the InGaN layers to be close to those expected from Vegard's law. Especially interesting are the results of Potin et al. [40] and Tran et al. [41] for QW structures. This can only be understood by considering the growth of these structures by the Stranski–Krastinov formation of islands that are elastically relaxed near the top surface during growth, as discussed in detail in Section 3.

Analysis of the thermodynamics of alloy formation for InGaN in complex, real structures, such as multi-quantum wells (MQWs) grown on sapphire/GaN substrates, is more complex than the calculations described above, which are for incoherent, bulk systems. First, the strain energy associated with coherent spinodal decomposition (the formation of In-rich regions that are coherent, i.e., having no mismatch dislocations at the interfaces where x changes) will suppress PS. This is because coherent In-rich regions are under significant compressive strain in a more Ga-rich matrix, which has a high energy cost for the system. This coherency strain is predicted to completely suppress spinodal decomposition in most III/V alloys [45]. Second, biaxial strain due to lattice parameter mismatch between the substrate and underlying layers on the InGaN layer under consideration also significantly affects spinodal decomposition. InGaN coherently grown on GaN is under compressive strain, since In atoms are larger than Ga atoms. This mismatch strain suppresses the formation of In-rich clusters, which have a larger equilibrium lattice constant than the matrix. Karpov [46] has calculated the InGaN phase diagram taking this strain energy into account for both zincblende and wurtzite structures. Since the strain energy is anisotropic, the magnitude of this effect depends on substrate orientation. The phase diagram of Karpov indicates that for InGaN grown coherently on GaN, spinodal decomposition will be nearly completely suppressed for typical growth temperatures. Thus, the fact that the layers analyzed by Ponce et al. [35] are incoherent is a vital factor. Similar, results were reported by Rao et al. [36] for thick layers. They reported that in the upper part of the layer, where the strain is relaxed by misfit dislocations, PS within the growth plane was clearly observed. For the part of the InGaN near the underlying GaN layer, the InGaN was coherent and spinodal decomposition was suppressed by the strain due to the lattice parameter mismatch. Thus, in comparing various experimental results, it is critical to consider thin, coherent epilayers separately from thick, incoherent layers.

In addition to these thermodynamic effects, kinetic effects must also be important in determining the size and the magnitude (Δx) of any compositional fluctuations due to spinodal decomposition. For alloys with compositions lying between the spinodes, shown in Fig. 2, where the alloys are unstable to a slight compositional fluctuation, the extent of the compositional fluctuations will increase during growth and will typically be kinetically limited, probably by surface kinetics since bulk diffusion is very slow in III/V semiconductors [47].

The detailed understanding of spinodal decomposition in thin, coherent epitaxial InGaN layers is further complicated by the coupling between the various individual phenomena, since strain and solid composition are mutually interdependent, as discussed above Eqs. (2)–(4) and the thermodynamic stability of the solid is a function of both strain and solid composition. To date, there have been no comprehensive calculations considering all of these factors. Such calculations would be expected to provide an important approach to gaining an increased understanding of these phenomena.

2.6. Stranski–Krastanov growth

Any understanding of these phenomena, as applied to the real InGaN materials used in the quantum wells of LED and laser devices, which will be the focus of this paper, requires analysis of the mechanisms of epitaxial growth at the microscopic level. For example, strained epitaxial layers in semiconductor systems are

normally found to grow by the Stranski–Krastanov (S–K) mechanism, involving the formation of a high density of small islands as well as a thin wetting layer [48,49]. This mechanism is expected to dominate the growth process for the InGaN quantum well structures used in blue and green LED devices, due to the large lattice parameter mismatch, and has been observed experimentally [25]. For example, a thin, lattice-mismatched, InGaN layer is grown on GaN and is subsequently covered by a second GaN layer.

Another possibility, based on observations for the epitaxial growth of strained SiGe layers is strain relaxation by the formation of pits or pinholes in an otherwise uniform, coherent epitaxial layer [50].

The phenomenon of S–K growth has been widely studied because the islands formed may constitute, when properly controlled, an array of quantum dots (QDs). This self-assembly process is a candidate as a practical technique for the fabrication of QDs for commercial injection laser devices. The reduced dimensionality of QDs gives rise to markedly superior device performance [51]. The S–K process for growth of a lattice mismatched epitaxial layer produces a series of islands, because the strain energy is lower for than for a uniform layer; thus, there is a thermodynamic driving force for island formation [48,52]. In S–K growth, a thin 1–2 ML uniform "wetting" layer is first formed by 2-dimensional (2D) growth on the substrate. As growth continues, an array of 3-dimensional (3D) islands forms spontaneously. The transition from 2D to 3D growth at a certain critical layer thickness has been observed for many semiconductor materials, grown by many techniques, as described below.

Among the first systems studied was the growth of Ge QDs on Si substrates. Strain-induced self-assembly of coherent islands was observed for Ge layers nominally a few monolayers (MLs) in thickness [53]. Of the III/V semiconductors, the growth of InAs and InGaAs QDs on GaAs has been perhaps the most widely studied. For example, Leonard et al. [54] found that $In_{0.5}Ga_{0.5}As$ coherently strained islands were spontaneously formed on (0 0 1) GaAs substrates by MBE after deposition of 4 ML of InGaAs. Moison et al. [55] studied the MBE deposition of InAs on GaAs. They found the transition from 2D to 3D growth to occur at a coverage of 1.75 ML. AFM measurements showed that islands 3 nm in height and 24 nm across were formed. The value of this self-assembly technique was shown by the remarkably uniform size of the islands formed. This is, of course, of vital importance for achieving the desired device performance. The OMVPE technique has been used to produce multi-layered QD structures in this system that have been used to produce injection laser devices with very low threshold current densities [51]. Interestingly, an early use of these InAs QD structures was to localize recombination in GaAs layers grown on Si substrates, where the high dislocation density kills the radiative recombination efficiency in homogeneous GaAs layers [56]. When the density of QDs exceeds the dislocation density, the InAs quantum dots collect the minority carriers for radiative recombination before they can reach a dislocation.

Another example of self-assembly via the S–K mechanism is the OMVPE growth of GaSb on GaAs substrates. For layer thicknesses of 4 ML, GaSb quantum dots are formed. Kinetic Monte Carlo simulations confirm that this is due to the strain induced by the lattice mismatch [57].

The S–K growth of island structures has also been observed for GaN on AlN. A 2D to 3D transition occurs after a critical thickness of approximately 3 MLs [8]. The GaN islands are truncated hexagonal pyramids with a height of 2–5 nm and a width of 10–30 nm. S–K growth is relatively easy for InGaN grown on GaN due to the large lattice mismatch of 11% between InN and GaN. Moustakas and co-workers [32] reported S–K growth of InGaN QDs on AlN by rf plasma assisted MBE. A transition from 2D to 3D growth occurred after the deposition of several MLs of InGaN on AlN. After 12 ML coverage, the average diameter and height of the InGaN islands, with $x=0.43$, were 30 and 3 nm, respectively. Yamaguchi et al. [58] reported the S–K growth of InGaN islands on GaN by both MBE and OMVPE. RHEED studies during MBE clearly showed a 2D to 3D transition as the InGaN layer thickness increased. For samples grown by OMVPE, the 2D to 3D transition occurred for layer thicknesses of 4–5 nm, with an In concentration of 0.22. The aspect ratio for the faceted, entirely coherent islands (no misfit dislocations) was found to be approximately 2. Pristovsek et al. [25] used *in situ* ellipsometry to study the thickness at the 2D–3D transition in InGaN layers grown by OMVPE as a function of the In composition. They found a value of approximately 1.5 nm for $x_{In}=0.20$ and a value of approximately 2 nm for $x_{In}=0.15$. InGaN QDs 1–2 nm in height and 40–50 nm in diameter have been observed to form by the S–K growth mode during OMVPE growth by Jung et al. [59]. Self-assembled InGaN QDs were also produced by atmospheric pressure OMVPE by Tachibana et al. [60]. They attributed the QD formation to PS in the InGaN.

There is a critical value of In content of the InGaN in order to provide sufficient mismatch to drive S–K growth. For MBE using NH_3, this critical concentration was found to be 12% [61]. However, this will be highly dependent on the growth technique and parameters such as temperature and growth rate as well as the layer thickness. Obviously, as the In concentration of the thin layer increases, the tendency to form S–K islands also increases. It should be mentioned that when the In concentration is very high, the islands become incoherent. InN quantum dots on GaN are not coherent: a network of dislocations is formed between the InN island and the GaN substrate due to the large misfit [62,63].

These important findings show that S–K growth may occur during the OMVPE growth of thin InGaN layers in MQW structures such as those used in LEDs and lasers. The size, composition, and distribution of the islands will certainly depend on the In content, layer thickness, and detailed growth conditions. The results cited above indicate that the InGaN S–K islands will be coherent, except for the growth of nearly pure InN quantum wells. This behavior is distinctly different that that expected for relatively thick layers, where dislocation generation results in relaxation of the strain due to lattice mismatch, perhaps inhomogeneously, which results in more complicated effects. This adds emphasis to the observation that in interpreting the wide ranging results found in the literature, it is important to consider phenomena observed in thick InGaN films separately from those in the thin QW structures used in light-emitting devices.

S–K growth was specifically demonstrated to occur for InGaN layers in MQW structures grown by OMVPE. In single quantum well (QW) structures used for LEDs, Florescu et al. [64] reported, for the 3 nm wells containing approximately 15% InN, 3D, i.e., S–K, growth, giving much enhanced 300 K photoluminescence (PL) intensities. The effects of inhomogeneous distribution of In on optical properties and device performance will be discussed in Section 3. For other examples of S–K growth in thin InGaN layers by both OMVPE and MBE, the reader is referred to Ref. [8].

Efforts have been made to control spinodal decomposition during QW growth, since it may be an important factor affecting device performance. One approach has been the use of anti-surfactants (Si in particular) in an effort to enhance QD formation during the S–K growth of InGaN on AlGaN by OMVPE [65]. For growth at 800 °C, Hirayama et al. produced InGaN QDs in an AlGaN matrix for layers 3 nm thick. The diameter and height of the QDs were reported to be 10 and 5 nm, respectively. Intense room temperature PL was reported. Other authors have inserted

buried layers to control the strain in the InGaN QW layer(s). This will affect both the mismatch strain in the QW layer(s) and the In incorporation, via the lattice pulling effect. Both will affect the formation of S–K islands. For example, Huang et al. [66] found enhanced emission efficiency for green InGaN/GaN QW LEDs when a pre-strained buried layer was added. Park et al. [67] used surface roughening to enhance PS in thin InGaN layers grown on GaN. The layer thicknesses were less than the critical thickness for strain relaxation, t_c. However, intentional surface roughening was believed to produce unstrained, incoherent S–K islands. In the layers with enhanced spinodal decomposition, they observed intense PL emission from the In-rich areas at significantly lower energies than the PL of the material grown on flat GaN layers. Other examples are given in Section 4, dealing with the production of single junction, white LEDs.

Lai et al. [68] used a 5 period InGaN/GaN MQW structure, grown by OMVPE at 780–880 °C, with 2 nm InGaN wells, sandwiched by GaN to produce materials emitting at wavelengths from blue into the yellow region of the spectrum. They characterized the samples using X-ray diffraction (XRD) and transmission electron microscopy (TEM), using sample preparation conditions specifically found to give no artifacts of the type discussed below. They reported PS to occur due to spinodal decomposition during S–K growth of the InGaN, resulting in the formation of In-rich clusters, coherent with the matrix, having very uniform diameters of 2 nm (medium In, green luminescence), 2.5 nm (high In, yellow luminescence) and 3 nm (low In, blue luminescence). As discussed in Section 4, the control of PS to produce yellow emission is important for the fabrication of single junction, white LEDs.

The analysis of the microstructure of InGaN in the QW structures used for light-emitting devices is obviously complicated by the fact that growth may occur by the formation of coherent islands. The driving force for the formation of the InGaN islands is a reduction in strain energy relative to that of a uniform InGaN layer containing the same number of In and Ga atoms [48,51]. Of course, this also increases the surface energy. Minimization of the total energy leads to an optimum size and shape of the self-assembled islands. Importantly, the island structure allows elastic relaxation of the epitaxial material at the island edges and, especially, the pyramidal apexes, without the generation of misfit dislocations. PS in these islands has not been analyzed for InGaN. However, for the similar GeSi/Si and GaInAs/GaAs systems, the gradient in elastic strain has been found to result in segregation of the larger alloy component to the apex of the pyramidal QD, due to lattice latching, as discussed in Section 3[69]. For InAs QDs formed on GaAs substrates grown by MBE, the nominally InAs islands are found to be composed of InGaAs. The compositional inhomogeneity of these islands has been experimentally investigated by Lamaitre et al. [70]. They found that the In content is largest at the apexes of the pyramidal-shaped islands. Cathodoluminescence (CL) studies of InGaN structures grown on GaN pyramidal islands have reported a distinctly higher In incorporation at the apexes of the pyramids, where the mismatch strain is relaxed elastically [71]. It is important to note that all of the relaxation discussed here occurs without the presence of misfit dislocations.

In terms of the basic thermodynamics, discussed above, several phenomena can be expected to lead to PS for the S–K growth of *thin*, coherent InGaN islands on GaN. First, strain will suppress spinodal decomposition in coherent thin layers, but this constraint will be relaxed non-uniformly in S–K islands. In addition, the elastic relaxation will give more In incorporation in the more strain relaxed parts of the islands, due to the lattice pulling effect. Both phenomena will result in PS, i.e., the formation of local In-rich regions during growth. For clarification, the term In-rich would be more precisely InN-rich, since the material in both phases is a nearly stoichiometric III/V semiconductor. The same PS phenomena would be expected to occur for the pits formed in a thin, strained layer [50], since elastic relaxation will occur near the pits, as for islands. However, only pyramidal growth will be addressed in the remainder of this paper.

In some instances, plastic relaxation of islands due to the introduction of misfit dislocations, as has been observed for small InN islands grown on GaN, will allow the islands to incorporate more In than expected for coherent layers and will also eliminate the strain suppression of spinodal decomposition and, thus, provide a third path to PS (the formation of In-rich clusters). This method is intentionally used to produce incoherent InGaN islands by roughening the surface [67]. When the QDs formed by this process are capped by a GaN layer, a QW layer with non-uniform In concentration is intentionally produced. This is one technique for the fabrication of white LEDs, as discussed in Section 4. However, the presence of misfit dislocations near the recombination regions may lead to increased non-radiative recombination.

Two other types of PS have also been observed specifically in thick layers ($t > t_c$), where mismatch dislocations are generated. A novel type of PS was recently reported for thick layers of both GaInP [72] and GaInN [25,36,73,74], where the initial, pseudomorphic, coherently strained part of the epitaxial layer has much less In than the later part of the epitaxial layer where the generation of mismatch dislocations has allowed plastic relaxation of the strain. Work by Pereira and co-workers [75] has suggested that for layers thicker than the critical layer thickness, t_c, (approximately 50 nm for x=0.17) the strain can become inhomogeneous, giving rise to regions having different bandgap energies, directly due to the inhomogeneous strain and, perhaps, to the resultant variation in In incorporation in regions having different amounts of strain. Pereira et al. [75] discussed their results solely in terms of the strain, but they did not rule out the more complex coupling of strain and solid composition. These complex phenomenon can give rise, in relatively thick layers ($>$50–75 nm), to a splitting of PL spectra and double X-ray scattering peaks [76]. This will not be discussed further, since these phenomena are expected to be absent in the layers of the MQW structures used for LEDs and lasers, where the layer thicknesses are typically approximately 2–3 nm, far less than t_c. Thus, in our efforts to interpret the results of optical, X-ray, and TEM results, in Section 3, mainly thin, coherent layers will be considered.

Several hundred papers have been written on the effects of the individual phenomena described above: strain effects, lattice latching, ordering, and spinodal decomposition. As a result, all of these phenomena are fairly well understood at the macroscopic level for uniform, either completely incoherent or coherent, epitaxial layers. However, few papers have described these phenomena in the coherent islands produced during S–K growth. The purpose of this paper is to present an integrated picture of these phenomena in an attempt to form a foundation for understanding the key materials issues that will determine the performance of InGaN alloys in device applications. What has largely been missing in the analysis of these results in the past has been a consideration of the coupling between the various phenomena as well as the critical role of S–K growth in the occurrence of these phenomena during growth.

In spite of all the complexities and potential pit-falls inherent in any attempt to understand PS in thin, coherent InGaN layers grown by OMVPE, it is worthwhile to make the attempt, since the occurrence of PS is certainly of critical importance for devices. PS will produce an emission wavelength in an LED or laser that is longer than expected for a random alloy because carriers collect in bandgap minima, so the emission energy is controlled by the local

In composition. In addition, there is a great deal of evidence that the formation of In-rich clusters produces a remarkable increase in radiative recombination efficiency in these highly dislocated materials, as discussed in Section 4.

3. Discussion of InGaN materials properties in terms of microstructure

Viewing key experimental results in the context of the basic materials phenomena reviewed above, it is possible to begin to analyze and make sense of claims and data found in the literature relating the microstructure to the materials properties of InGaN. However, in examining the data it will be vital to separate the effects of inhomogeneities in plastic relaxation of strain and solid composition for thick layers ($t > t_c$) from inhomogeneities in alloy composition and elastic relaxation of strain for thin, coherent QW layers.

Consider first the thick layers that are relaxed by the formation of misfit dislocations. The experimental evidence from XRD, TEM and CL for thick (0.1–4 μm) GaInN layers grown by OMVPE indicate that incoherent spinodal decomposition occurs. The data shown in Fig. 2 are in close agreement with the calculated phase diagram, which does not include the effects of strain.

Peirira and co-workers [75] reported evidence that for thick InGaN layers, inhomogeneous *plastic* relaxation of the strain due to non-uniform lattice misfit dislocation formation may directly give variations in bandgap energy and/or give rise to In clustering due to enhancement of In incorporation in more relaxed regions, due to lattice pulling. Both factors may cause splitting of optical emission spectra and the doubling of X-ray peaks.

The emphasis here is on the thin layers, $t \ll t_c$, used in MQW LEDs and lasers, with thicknesses of 2–3 nm and In mole fractions of 0.15 and 0.20. For these layers inhomogeneity in In composition is more likely a result of either spinodal decomposition or the inhomogeneous *elastic* relaxation of mismatch strain, for example at the apex of a pyramid-shaped island. This will result in increased In incorporation due to lattice pulling, as described in detail in what follows.

Clearly, there are a number of mechanisms that will give PS in InGaN epilayers. For the thin, coherent InGaN structures used in QW LEDs, it is first necessary to deal specifically with the expectation that spinodal decomposition cannot occur in InGaN layers due to its suppression by strain in a totally coherent system [77]. As discussed above, spinodal decomposition is inhibited by strain due to the production of high energy, strained clusters in all III/V alloys where the atoms on the sublattice where mixing occurs have different covalent radii. However, this is based on the assumption that the material under consideration is in the bulk. The systems will behave differently when in the form of thin films, where the surface plays a significant role. In a classic paper, Glas [78] extended the work of Stringfellow [45], on strain stabilization, described above, to include relaxation at the free surface of the layer and the composition pulling effect, also described above. He showed that for a thin, coherent epitaxial layer, these effects lead to calculated critical temperatures for PS much larger than for the bulk. These predictions have been verified experimentally, as for instance in the beautifully detailed study of McDevitt et al. [47] for InGaAsP epitaxial layers grown on several substrate orientations by LPE and MBE. They show that 2-dimensional PS occurs anisotropically near the surface during epitaxial growth of thin layers of InGaAsP, where the simple strain stabilization theory [45] would predict that spinodal decomposition should not occur.

In order to encompass our current understanding of the epitaxial growth of thin layers, the effects of elastic relaxation in S–K islands must also be included in this analysis. The misfit strain relaxation in an island will be considerably greater than at a free, flat surface, since the island can relax laterally. In addition, the sublayer beneath the thin layer will relax under an island [48]. This means that spinodal decomposition will be much more likely to occur during island growth, particularly near the top of the island where the material is the most relaxed.

Consider the growth of coherent, pyramid-shaped S–K islands. This has been analyzed for the heavily studied Si_xGe_{1-x} islands on Si and for $Ga_{0.5}In_{0.5}As$ islands on GaAs. For example, Medhekar et al. [69] considered the coupled effects of solid composition, solution thermodynamics, mismatch strain, and island shape on the composition maps of both GeSi and InGaAs islands at thermal equilibrium. Their calculated results show the dependence of phase separation in individual islands, termed the segregation index, Φ,

$$\Phi(F_o, \vartheta) = 4/V\left(\int [c(x) - c_{avg}]^2 dV\right) \quad (5)$$

on the pyramidal angle, ϑ, and the ratio of the free energy of mixing to the elastic energy density, F_o. In this equation, V is the volume of the island, $c(x)$ is the local concentration, and c_{avg} is the average concentration. Their results, reproduced in Fig. 3, show that the PS increases for both large values of ϑ and for alloys with a driving force for spinodal decomposition, where F_o is positive, as it is in InGaN at normal growth temperatures. Φ is 0 for a completely compositionally uniform island and 1.0 for an island composed entirely of two phases with compositions 0 and 1.0. Of course, even for complete PS, giving the two compositions x_1 and x_2 (see Fig. 4(b)), Φ could never be as large as unity. For example, for an overall average concentration of 0.5, if $x_1 = 0.15$ and $x_2 = 0.85$, $\Phi = 0.5$. Clearly, a large amount of PS is expected for InGaN islands grown at temperatures below the critical temperature for spinodal decomposition, where F_o is positive, although the island shape will be important. These calculations were done for pyramidal shaped islands. This assumption will be adopted in the remainder of this section.

Calculations of Jalkanen et al. [79] show that, as intuitively expected, for tall (relative to the width) pyramidal shaped islands,

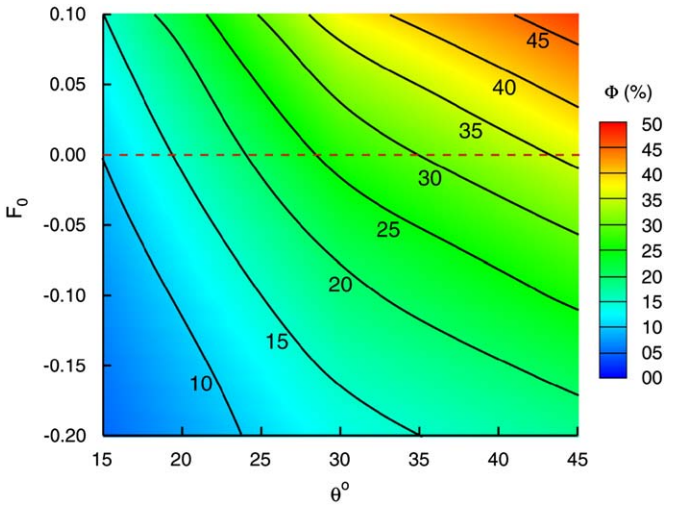

Fig. 3. Compositional phase diagram showing the degree of segregation, Φ, as a function of the parameter F_o and the shape of the quantum dot crystal represented by the angle of the pyramidal sidewalls, θ. Even when the thermodynamic mixing energy favors mixing ($F_o < 0$), the relaxation of strain for quantum dots with steep sidewalls results in alloy segregation within the quantum dot. Even when the thermodynamics favors phase separation ($F_o > 0$), complete decomposition is not observed. The average composition of the quantum dot c_{avg} is 0.5 (after Medhekar et al. [69]).

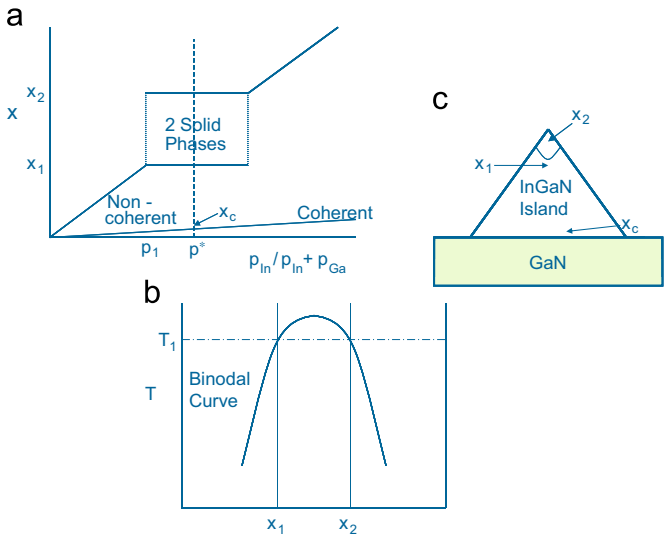

Fig. 4. Illustration of composition profile for pyramidal S–K islands at equilibrium for input temperature, T_1. (a) In concentration in the solid versus input partial pressure of the In precursor/total group III partial pressure; (b) T–x phase diagram showing solid phase miscibility gap; (c) schematic diagram of composition profile for a hypothetical pyramidal InGaN island grown coherent with the underlying GaN layer for an input partial pressure of In precursor/total group III partial pressure of p^*. The solid line indicates an abrupt transition from the binodal In-rich phase, x_2, to the 2nd equilibrium phase, x_1.

elastic relaxation in the region near the pyramidal apex is almost complete. This makes the analysis of InGaN islands relatively simple. Assuming that the entire island is in equilibrium with the vapor, an assumption that will be re-examined below, and that the relaxation at the base of the pyramid is minimal, the thermodynamic equations giving the solid composition at the base of the island and at the apex are exactly the same as those used to compare the composition of a thin coherent layer and an incoherent island [18]. For the region near the top of the pyramid (shown in Fig. 4(c)), the In content of the solid, x_2, is obtained by solving the two equations

$$\mu^v_{\mathrm{In}} + \mu^v_{\mathrm{N}} = \mu^s_{\mathrm{InN}}(\text{strain-free top of island}) \tag{5a}$$

$$\mu^v_{\mathrm{Ga}} + \mu^v_{\mathrm{N}} = \mu^s_{\mathrm{GaN}}(\text{strain-free top of island}) \tag{5b}$$

where the chemical potential of the solid (μ^S) has only the standard entropy and enthalpy of mixing terms [13]. For the bottom of the island, where the lattice is compressed to have nearly the same lateral spacing as the underlying GaN, the equations are similar, but in this case the chemical potential terms for the solid will contain an elastic energy term

$$\mu^v_{\mathrm{In}} + \mu^v_{\mathrm{N}} = \mu^s_{\mathrm{InN}}(\text{strained bottom of coherent island}) \tag{6a}$$

$$\mu^v_{\mathrm{Ga}} + \mu^v_{\mathrm{N}} = \mu^s_{\mathrm{GaN}}(\text{strained bottom of coherent island}) \tag{6b}$$

The line labeled "coherent" will give a value of x_c, in Fig. 4(a) that is much lower than the equilibrium concentration for the relaxed solid. The ratio of the In concentration at the apex to that at the base, $x_{\mathrm{apex}}/x_{\mathrm{base}}$, will be approximately $1/Q$, from Eq. (4), a number of the order of 10. This is shown schematically in Fig. 4(a), where the In mole fraction in the solid (x) is plotted versus the input partial pressure of In divided by the total group III partial pressure, typically $p_{\mathrm{TMIn}}/(p_{\mathrm{TMIn}}+p_{\mathrm{TMGa}})$. The slope of the line labeled "non-coherent" is determined by the In distribution coefficient, a number that is nearly unity, but which decreases at high temperatures, as discussed in Section 2 (a).

The inclusion of the thermodynamic instability of InGaN due to spinodal decomposition at temperatures below the critical temperature can be easily included by assuming that PS can occur when the coherency strain is elastically relaxed, near the top of the pyramid. It will be completely suppressed by the mismatch strain in the region near the base. The result is included in Fig. 4(c), taking the two binodal points at the specified temperature (from Fig. 4(b)) as x_1 and x_2, in order to make the diagram specific and clear. For typical InGaN growth temperatures the numbers would be approximately 0.05 and 0.95, as discussed in Section 2(e).

To clarify the diagram, let us consider the sequential growth of InGaN islands with gradually increasing values of p_{TMIn}. At low In partial pressures, the solid composition at the top of the pyramid will be given by the line labeled "non-coherent". This solid composition is in the single solid phase region of Fig. 2, the actual InGaN phase diagram. At the base of the pyramid, the solid composition will be given by the point x_c on the lower line of Fig. 4(a) for a thin coherent layer. As the In partial pressure increases the amount of In in the solid at the two points within the island will simply follow the two lines, with approximately $10x(1/Q)$ more In incorporated at the top than at the bottom of the island. When the value of In partial pressure exceeds a certain value, p_1 in the schematic diagram, Fig. 4(a), the system will enter the two phase region of the T–x phase diagram. Since there are now two solid phases in equilibrium with the vapor, the system becomes thermodynamically invariant [13]. This means that with increasing In partial pressure two solids are formed, with compositions, x_1 and x_2, with compositions that will not change as p_{TMIn} increases. They will depend only on temperature. The only change will be in the ratio of the amounts of the two phases. In contrast, at the base of the pyramid, the solid composition will continue to increase with increasing In partial pressure, along the "coherent" line. The In partial used for the growth of the quantum wells for commercial blue and green LEDs is represented in this diagram as p^*, since the In content will exceed x_1 or 5% in the actual T–x diagram for InGaN. The result is that spinodal decomposition will occur near the top of the pyramidal island for the normal In concentrations used for the growth of the blue and green LEDs. The composition profile is shown schematically in Fig. 4(c) for such an island at equilibrium with the vapor. The In-rich phase, with concentration x_2, will be formed near the apex of the pyramid and the Ga-rich phase, with concentration x_1, will be formed just below. An abrupt transition between x_1 and x_2 is indicated by the solid line. The In content will decrease continuously as the position moves closer to the base of the pyramid, due to the increasing influence of strain from the underlying GaN. At the base, the In content of the solid will be x_c. Of course, spinodal decomposition will not occur in the region near the bottom of the pyramid because the In content will be low and the strain from the underlying GaN will suppress spinodal decomposition. In this case, where equilibrium is established throughout the island, the strain in the InGaN due to the underlying GaN will be small, i.e., the island will have little biaxial strain. Thus, the strain gradient will be small even though the gradient in solid composition may be large.

The above analysis has assumed equilibrium between every part of the island and the vapor. We are not certain that this is completely valid, since the diffusion coefficients of In and Ga in the solid are extremely low, even at the growth temperatures of the InGaN. Another approach would be to assume that the In distribution in the island at the surface at any one time during island growth is determined thermodynamically and that it is then frozen during growth of the remainder of the island, i.e., that no In transport within the island is allowed. This case has been analyzed for InGaAs islands grown on GaAs [80]. It also results in In accumulation within the island, but rather than just at the apex of the pyramid, the In-rich region is formed near the apex for each succeeding layer of the island as growth progresses. This results in

an inverted-triangle shaped, In-rich core. In this case, for a core with In content that is within the region of the miscibility gap, spinodal decomposition would occur near the apex of the pyramid, where the coherency strain is elastically relaxed. Thus, this analysis would also predict the In-rich second phase to form at the pyramidal apex. However, in this case, the In content at the center of the base could also be much larger than x_c. It is expected that spinodal decomposition in this region would again be suppressed by the coherency strain induced by the underlying GaN layer.

Either of these analyses, for equilibrium within the island or for a frozen-in In distribution, gives a process for the self-assembly of a series of In-rich clusters with a density equal to the density of islands, which has been reported to be as high as 10^{12} cm^{-2} in InGaN grown on GaN by OMVPE [81]. Importantly, when the island density is greater than the dislocation density, typically of the order of 10^8 cm^{-2} in high quality epitaxial layers [7], the In-rich regions will capture the injected minority carriers in an LED where they will recombine radiatively before they can reach dislocations, where they would recombine non-radiatively. This will be discussed in much more detail in Section 4, where LED performance is considered.

As a brief aside, this analysis accounts for the In-clustering widely observed in InGaN layers, as discussed below. However, another explanation for the localization of exciton recombination is the formation of In–N chains [77,82]. This explanation has gained recent popularity due to the assumption that spinodal decomposition cannot occur in thin, coherent InGaN layers. However, as discussed above, this is clearly not correct. There is no reason to rule out the effects of In–N chains, which are energetically stable; however, they have not been observed experimentally. Furthermore, it seems unlikely that the presence of In-N chains could account for a stokes shift of 570 meV, as discussed in Section 3.5, below.

The growth temperature will have a large effect of the density and size of S–K islands. For kinetic reasons, low growth temperatures give a higher density of smaller islands [60]. Of course, other growth conditions, particularly the growth rate, will also have major effects on the island size and density. For MBE growth, island densities of 10^{11} cm^{-2} have been reported, similar to those observed for OMVPE growth [81,83].

One other possibility must also be considered before leaving this topic. In the case where the island is formed directly above a dislocation in the underlying layer or mismatch dislocations are formed for any reason, the analysis must be quite different. Since for relatively large islands, the free energy of an incoherent island will be lower than that of a coherent island [48], these islands would be expected to grow more rapidly. Furthermore, surrounding small islands will donate their atoms to the larger island. This might be an explanation for the bimodal S–K island size distribution observed for InGaN [60]. In fact, for MBE growth, Moustakis et al. [32] observed just such a phenomenon. It might also account for the possible accumulation of In in regions near threading dislocations [64,84,85]. Plastic relaxation of the mismatch for an island formed at a dislocation would provide a mechanism for producing an In-rich region adjacent to the dislocation. The deliberate relaxation of the coherency strain energy has been produced by growth of InGaN on a roughened GaN sublayer. This was reported to allow the spontaneous formation of relaxed InGaN QDs [67]. Since these islands have been relaxed by the generation of misfit dislocations, there is no driving force to produce a non-uniform In distribution; thus, they would be expected to have a uniform composition.

At this point, it is worth reiterating the statement made above that in addition to the thermodynamic factors, the likelihood of spinodal decomposition during epitaxial growth is also expected to depend critically on kinetic factors that will be dependent on the growth technique and the detailed growth parameters. It is unknown whether thermodynamic equilibrium will, indeed, be obtained during the very short growth time for InGaN layers in MQW LED and laser structures. It is likely that the In content of the In-rich regions formed during growth will not always have the high In content predicted in Fig. 2.

For simplicity, in what follows the discussion will address mainly PS in thin InGaN layers. The term PS will include any process, including spinodal decomposition or lattice pulling in S–K islands to produce a non-uniform alloy composition, in particular the small, In-rich regions observed for InGaN layers grown by OMVPE under certain conditions. Formation of these In-rich regions is found to play an important role in improved device performance, as described in Section 4. PS has been observed in InGaN layers, particularly the thin InGaN well layers in quantum well structures grown by OMVPE. A non-inclusive list of techniques giving evidence of PS in these layers includes: X-ray techniques, Raman scattering, TEM, CL, and optical techniques. These experimental results will be reviewed in the following sections.

3.1. X-ray fine structure (EXAFS)

Perhaps the most easily interpreted evidence of the non-uniform In distribution in InGaN layers is obtained from X-ray fine structure (EXAFS) experiments. X-ray fine structure analysis can be used to "count" the number of In-In neighbors for comparison with the number expected for a random distribution of In and Ga atoms on the cation sublattice. Kachkanov et al. [86] clearly showed that the In distribution in InGaN is not random. An excess of In–In pairs indicates the formation of In-rich regions in epitaxial layers with In contents of less than 0.4 grown by either MBE or OMVPE. They were able to correlate that presence of In-rich clusters to an increase in radiative recombination efficiency due to localization of exciton recombination to InN-rich regions [86] "in short, the result indicates the existence of InN-rich regions in InN-poor material and with In fractions of less than 40%, excitons are localized on InN-rich InGaN regions". This work is somewhat difficult to analyze in terms of the basic materials factors discussed above, due to the lack of information about the layer thicknesses. The results of Miyanaga et al. [87] used EXAFS to study the In atom distribution in SQW structures, typical of those used in InGaN blue, green, and amber LEDs with x_{In} values of 0.145, 0.2, and 0.275, respectively. Their results indicate that the atomic distribution is random in the horizontal direction, but with In-rich aggregates in the vertical direction. O'Donnell et al. [88] also reported that this technique showed phase segregation in InGaN.

3.2. Raman spectroscopy

Raman spectroscopy has been used to study PS in thick InGaN layers. Lemos et al. [89] used resonant Raman scattering to study layers of cubic InGaN produced on (0 0 1) GaAs substrates by MBE. They interpreted the spectra obtained for samples with x ranging from 0.07 to 0.33 to the formation of an In-rich phase during growth. Similar conclusions were deduced from Raman spectra for the more typical 500 nm thick wurtzite InGaN layers grown by OMVPE with In contents ranging from 0.06 to 0.36 [38]. These results are consistent with the EXAFS results described above.

3.3. Transmission electron microscopy

TEM is a powerful technique for directly imaging the strain produced by formation of nanometer-scale, In-rich clusters in very thin layers. Since the wavelength of electrons is much smaller than for visible photons, the resolution of electron microscopes can be made so small that individual atoms can be resolved. This spatial resolution is much better than for other techniques. Thus, careful high resolution TEM gives the best evidence of the formation of In-rich clusters and, in particular, the size of the In-rich regions. Samples with In clustering are easily distinguished from those having a random distribution of In and Ga atoms.

The first TEM results were reported by Chichibu et al. [90] and Narukawa [91]. They showed clear evidence of the spontaneous formation of a high density of tiny In-rich QDs in the MQW structure of an LED. Since this time, there has been a shadow cast over these, and similar, early results. Smeeten et al. [92] suggested that apparent In-rich regions can be the result of artifacts produced during TEM sample preparation. Thus, they called into question all previous work. Any study of this sort cannot, of course, invalidate earlier work, but only suggests that in some cases artifacts may complicate the interpretation of the experimental results. Since the study of Smeeten et al. was published, the results of a number of careful studies that eliminated the possibility of artifact formation have been published that support the earlier results. Potin et al. [40] used high resolution TEM (HRTEM) to image single quantum well InGaN/GaN samples grown by both MBE and OMVPE. Their procedures avoided the formation of artifacts during sample preparation. They also used digital analysis of lattice images to determine the local In concentrations. They found In-rich clusters between 2 and 4 nm in diameter in the OMVPE sample. The maximum In concentrations measured in the In-rich phase were 42%, about twice the average In concentration of 21%. They mention that they always saw small In-rich clusters in each of the large number of samples grown by OMVPE. After considering various alternatives they concluded that the In-clusters are formed in the early stages of spinodal decomposition, due to the miscibility gap, during epitaxial growth.

Bartel et al. [93] describe very careful and detailed HRTEM studies of InGaN showing conclusively the presence of In-rich clusters in both bulk $In_xGa_{1-x}N$ ($x > 0.1$) samples and in quantum wells, with the thin InGaN layer sandwiched between higher bandgap barrier layers. In these studies, the amplitude of the compositional variation due to spinodal decomposition was found to be from $\Delta x = 0.1$ to 0.15 and the spacing between In-rich clusters was determined to be 2–4 nm. This can be compared to the distance between dislocations of 1000 nm for a dislocation density of $10^8\ cm^{-2}$.

Careful studies of the effects of TEM sample preparation conducted by Bartel et al. [94] showed that with proper thinning techniques, artifacts do not influence the results. This study showed that compositional fluctuations do, indeed, occur in InGaN quantum well samples. The indium fluctuations detected from lattice images, Z-contrast images, and local bandgap measurements were attributed to spinodal decomposition.

Jimschek et al. [95] reported the results of careful, analytical HRTEM measurements performed on the QW structures, with x_{In} approximately equal to 0.20, used in commercial green LEDs. Sample preparation was optimized to avoid the artifacts discussed above. This work demonstrates the presence of In-rich clusters 1–3 nm in size, surrounded by areas of excess Ga, consistent with spinodal decomposition of the InGaN. Imaging the local bandgap variation, they observed strong recombination at low bandgap, In-rich areas. This led to suppression of non-radiative recombination at dislocations, which were present with a high density of $2 \times 10^{10}\ cm^{-2}$ in these devices.

Kisielowski et al. [96] also used HRTEM to demonstrate PS for x_{In} values between 0.2 and 0.8 in InGaN, as expected from the phase diagram shown in Fig. 2. The spacing of the In-rich regions was 2–5 nm, similar to the values reported by Jimshek et al. [95]. In an earlier paper from the Berkeley group, Bartel et al. [97] studied the elimination of artifacts and reported spinodal decomposition in InGaN quantum wells used in commercial LEDs. These results are very similar to those published earlier by Chichibu [90] and Narukawa [91].

Clearly, when proper thinning techniques are employed, In-rich regions can be unambiguously imaged using TEM. The size of the In-rich regions is approximately 2–4 nm and the spacing is approximately 10 nm. Perhaps the most dramatic example that the TEM results are not always tainted by artifacts is the work of Park et al. [67] who examined two InGaN layers of the same thickness and solid composition, one grown on a smooth GaN "substrate" and other on a roughened GaN surface. The TEM results clearly show that the layer grown on the roughened substrate exhibits the In-rich regions due to PS and the layer grown on the smooth substrate does not. It seems very unlikely that this result is due to the formation of artifacts in one sample and not in the other.

The size of the In-rich clusters (2–4 nm) is important. The studies of S–K growth have reported island sizes approximately an order of magnitude larger, as discussed above. Thus, the PS is occurring only in certain parts of the islands, presumably the regions near the top, where the mismatch strain is allowed to relax.

3.4. Cathodoluminescence

The optical properties of the InGaN alloys can be used to provide additional information about the microstructure produced during OMVPE growth. Cathodoluminescence (CL), a technique where, minority carriers are excited using a highly focused electron beam in a TEM, allows imaging of the regions producing photons of a given wavelength. However, the spatial resolution for this technique is limited to the order of the minority carrier diffusion length [98], no less than 50 nm. Thus, it is impossible to give an accurate assessment of the size of the In-rich regions. Several CL studies have shown a non-uniform distribution of photon energies, i.e., small regions are seen to produce lower energy photons that the matrix. This is usually interpreted as due to the non-uniform distribution of In, in particular the formation of In-rich regions, in thin InGaN layers grown on GaN.

Early studies of Chichibu and co-workers [99] used CL mapping of QW LED structures to show the presence of quantum-disks, due to In clustering, which produce effective bandgap variations. The lower energy, tail states, were observed to originate from the In compositional inhomogeneity. The same group [100] used CL to confirm that the carrier localization originates from the effective bandgap inhomogeneity due to the clustering of In.

As discussed above, Ponce et al. [35] used TEM and CL together for a careful study of thick InGaN layers. For low In concentrations, they observed homogeneous material, as shown in Fig. 2. Beginning for In concentrations of approximately 0.1, they observed regions of higher In concentration. They concluded that the In clustering occurs only near dislocations. This is generally consistent with the phase diagram of Ho and Stringfellow that indicates such compositions should be metastable. For In concentrations of > 0.20, wide-spread PS was seen, indicative of the In clustering expected from spinodal decomposition.

The combined results in Fig. 2 appear to be in both qualitative and quantitative agreement with the calculated phase diagram. This was somewhat unexpected since, as discussed above, factors such as elastic strain and surface effects must be included in a complete analysis of PS in the InGaN system. A simple interpretation of the results is that for thin layers growth occurs by the S–K mechanism and that elastic relaxation of the islands occurs during growth which allows spinodal decomposition to occur as in an incoherent system. Apparently, in thick layers, incoherent spinodal decomposition may occur.

The Ponce group used time resolved CL spectroscopy to study InGaN (x_{In}=0.13) quantum wells grown by OMVPE. They found a distinct difference in behavior between thin (6 nm) and thicker quantum wells. For the thinner quantum wells, the behavior was found to be due to fluctuations in In content, which give rise to localization effects on electron–hole recombination [101]

Kyono et al. [84] showed very clearly and directly, using CL, that In compositional fluctuations decrease the non-radiative recombination at dislocations in AlInGaN 2.5 nm double QW structures used for UV LEDs. They found that with 6% In, there was no difference in PL intensity between layers grown on sapphire and those grown on GaN. This was interpreted to show that the presence of a significant concentration of In "passivates" the non-radiative recombination at dislocations. Furthermore, the CL images indicate that the dark regions surrounding dislocations, due to non-radiative recombination at the dislocation, disappear at In concentrations of 6%. This was attributed to the compositional fluctuations that collect minority carriers before they can recombine at dislocations. Similar results for InGaN QWs were attributed to PS at or near dislocations [102,103]. These results are in accord with the results of Srinivasan et al. [104] obtained for thick layers of InGaN, where a low energy emission in CL was identified as emanating from the regions near defects, such as dislocations.

In clustering is enhanced by annealing the InGaN samples. In this case, CL images of In-rich clusters are seen that emit yellow luminescence in contrast to the blue emission from the background matrix. An additional feature of the CL studies is the observation that the photons emitted in CL (as for photoluminescence (PL) or electroluminescence (EL)) have significantly lower energies that the photons necessary to excite the PL (so-called PLE spectroscopy). This is consistent with the EL spectra emitted by MQW LEDs, where spinodal decomposition is enhanced by the selection of favorable growth parameters. Emission from regions having two distinct bandgaps is observed in the same material. They were attributed to recombination from the In-rich clusters and the matrix [41]. The peak separation is related to the Stokes shift, discussed in the following section.

3.5. Optical properties—Stokes shift

A useful method of characterizing the non-uniform solid composition in InGaN layers is the so-called Stokes shift. Often a major luminescence peak (CL, PL, or EL) is observed at energy considerably lower than the bandgap energy, i.e., the energy for the onset of absorption. This is because the excited carriers, created by absorption in the matrix, can diffuse to the In-rich, lower bandgap regions before they recombine, giving photons with energies lower than the bandgap of the matrix. The Stokes shift is intimately connected to the appearance of dual emission peaks in CL, PL, and EL, discussed in the last section, since the two emission peaks can originate from the matrix and the In-rich areas.

Experimental values of the Stokes Shift are plotted in Fig. 5 versus the bandgap energy. It is seen that the value increases nearly linearly as the In content of the InGaN increases, from zero for GaN, to as much as 570 meV for material with an In

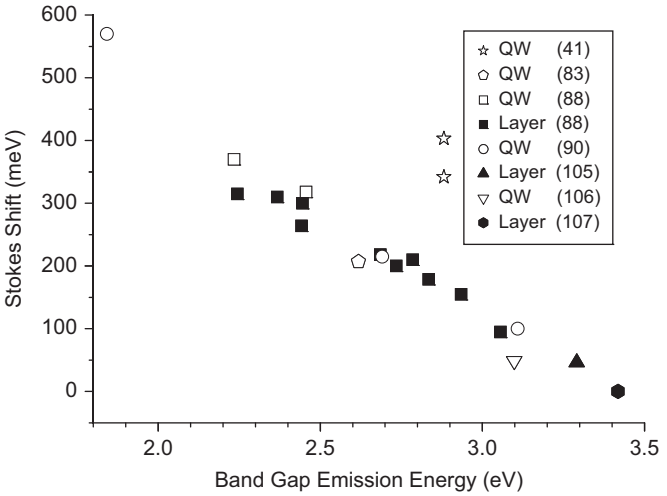

Fig. 5. Stokes shift versus bandgap energy for InGaN. Data for thick layers were taken from Refs. [88,105,107]. Data from QW samples were taken from Refs. [41,83,88,90,106].

concentration of 0.45. The Stokes shift obtained from the data of Tran et al. [41] for the separation of PL and EL peak energies, discussed above, appears to be considerably larger than the other data. The Stokes shift disappears for GaN, where there can obviously be no compositional variation, and increases systematically as the In content increases (the emission energy decreases). The scatter in the data suggests that the extent of fluctuation in In content is somewhat dependent on the growth conditions, as expected.

As discussed Section 2, for layers with thickness greater than t_c, the Stokes shift has been interpreted as at least partially due to an inhomogeneous distribution of strain [75,76].

However, the main focus of this paper is the thin layers used in MQW LEDs. For layers with thicknesses below t_c, Pereira et al. [75,76] reported no Stokes shift. However, many other researchers have seen a Stokes shift that increases with increasing In concentration, often specifically for the thin layers in MQW LEDs [41,83,88,90,106,108–112]. Chichibu et al. [90] compared the EL spectra with the photovoltage versus photon energy scans for MQW blue and green LED samples. They observed Stokes shifts of 100, 215, and 570 meV for In concentrations in the QW of 0.2, 0.3, and 0.45, respectively. Significantly, as seen in Fig. 5, the Stokes shift appears to be virtually the same for thick layers and for the MQW LEDs. This result is similar to that reported by O'Donnell et al. [88], whose data are included in Fig. 5, who found the Stokes shift for epilayers to be essentially the same as for commercial MQW LEDs.

As discussed in Section 2.6, S–K growth of lattice mismatched islands is expected to produce structures where the coherent islands have an inhomogeneous distribution of solid composition. In this scenario, minority carriers will collect in the low bandgap (high InN concentration) regions near the tops of the islands where they will give rise to photons having a significantly lower energy than the bandgap of the matrix, as indicated schematically in Fig. 6. However, the PL or CL peak energy cannot easily be used to directly determine the solid composition of the In-rich parts of the islands due to the quantum size effect as well as the quantum confined Stark effect (QCSE) in these rather complex structures.

3.6. Photoluminescence

PL uses the absorption of light ($h\nu > E_g$) to generate electron–hole pairs in the epitaxial layer. The minority carriers generated

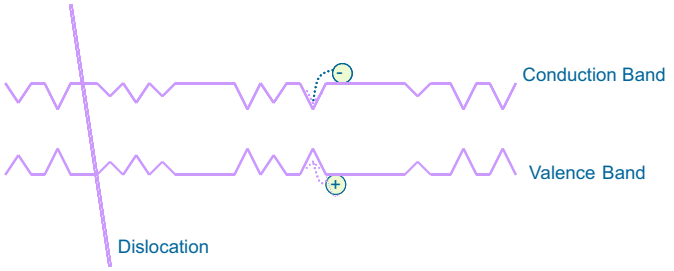

Fig. 6. Schematic illustration of fluctuations of energy bands due to In compositional fluctuations and their effect of minority carrier recombination.

diffuse a certain distance in the semiconductor and then recombine to produce light. For samples with PS resulting in In-rich clusters, which have a lower bandgap energy than the matrix, they are mainly collected in the smaller bandgap regions, as shown schematically in Fig. 6. PL may also be generated in the matrix. The difference in the energies of the 2 PL peaks (the Stokes shift) gives an indication of the extent of PS as discussed in Section 3.5. One complication is that deep levels in the InGaN may also produce a low energy PL peak. Thus, for this technique to convincingly show that the low energy emission is due to In-rich regions, rather than deep-level defects, it is vital to show that the PL does not "saturate" at high excitation intensities. Saturation at high excitation intensities would be indicative of PL due to recombination at imperfections or defects in the material. Tran and co-workers [41] examined the PL in MQW samples, with 3 nm InGaN layers having In concentrations of 22% for high brightness LEDs grown by production scale OMVPE. A clear splitting of the PL due to recombination in the matrix, at 2.881 eV, and in In-rich clusters, at 2.539 eV was observed. The Stokes shift was measured in this way to be 342 meV, which is included in Fig. 5. These authors convincingly demonstrated that the low energy PL peak does not saturate, which they interpreted to mean that the low energy PL originates from compositional fluctuations due to PS. The EL from these LEDs shows that the intensity of the lower energy peak does not saturate as current density increases. The Stokes shift measured from the difference in EL peak energy is also included in Fig. 5. An important point made in this paper is that the PS, leading to the formation of In-rich clusters, is strongly dependent on the conditions used for the growth of the MQW structures, indicating the importance of kinetic factors, as noted above.

3.7. Summary

Based on the theoretical analysis, it is clear that PS can occur in S–K islands of InGaN grown on GaN. The two mechanisms for PS in coherent islands are spinodal decomposition and composition pulling, both of which will produce non-uniform islands that are enriched in InN near the top. The experimental evidence for the occurrence of PS in thin layers is overwhelming. EXAFS studies show the formation of non-random In distributions, characteristic of In clustering. Accounting for potential artifacts, high resolution TEM clearly shows a very high density of 2–4 nm In-rich regions. The CL and PL splitting as well as the Stokes shift are consistent with the formation of In-rich regions in a more Ga-rich matrix.

4. LED performance

The inhomogeneous In distribution due to PS is of more than academic interest. Formation of In-rich clusters is found to have profound effects on the performance of laser and LED devices. As mentioned above, one of the great mysteries of the performance of InGaN blue and green LEDs is that the efficiency should be so high in materials with extremely high dislocation densities. In typical III/V alloys, dislocations have a strong deleterious effect on LED efficiency [9,10]. However, in InGaN, high efficiencies are obtained even for highly dislocated material. Chichibu et al. [90] were the first to explain this mystery in terms of localization of recombination at the In-rich clusters. Essentially, minority carriers are collected in the small bandgap regions at the In-rich clusters before they can recombine at dislocations, as shown schematically in Fig. 6. This yields an enormous increase in radiative recombination efficiency if the distance between the In-rich regions is smaller than the dislocation spacing. The S–K island density has been measured to be from 10^{10} to 10^{12} cm^{-2}, depending on growth conditions, which is orders of magnitude higher than the dislocation density in the high quality material used for high efficiency LEDs. Amazingly high values of external efficiency exceeding 60% have been reported for blue MQW LEDs in materials with extremely high dislocation densities, exceeding 10^7 cm^{-2}[113]. The dramatic increase in the external quantum efficiency as In is added to GaN in MQW LEDs is seen in Fig. 7 [114,115]. A small concentration of In gives a dramatic boost in LED efficiency. Indeed, it is impossible to produce high efficiency LEDs without the addition of In. The onset of this beneficial effect appears to coincide with some of the theoretical calculations, discussed in Section 2.4, which indicate the onset of PS for InN concentrations as low as 2%. However, considering the data on PS discussed above, it is surprising that the improvement in LED efficiency occurs at such low values of x_{In}. This may indicate that In–N chains form at these low In concentrations and cause localization of recombination.

The cause of the high quantum efficiency in materials with enormous dislocation densities is nearly universally acknowledged to be related to PS, producing low bandgap InN-rich clusters. However, as mentioned above, there have been other proposed explanations, including repulsion of minority carriers from dislocations, perhaps due to fluctuations in either composition or the quantum well thickness near dislocations, and/or the formation of In–N chains, which provide localized high exciton recombination rates. Certainly, doubt is cast on these explanations based on the fact that the Stokes shift can be as large as 570 meV and the increase in recombination efficiency is observed in thick layers as well as in quantum wells. In addition, the temperature dependence of radiative lifetime gives conclusive

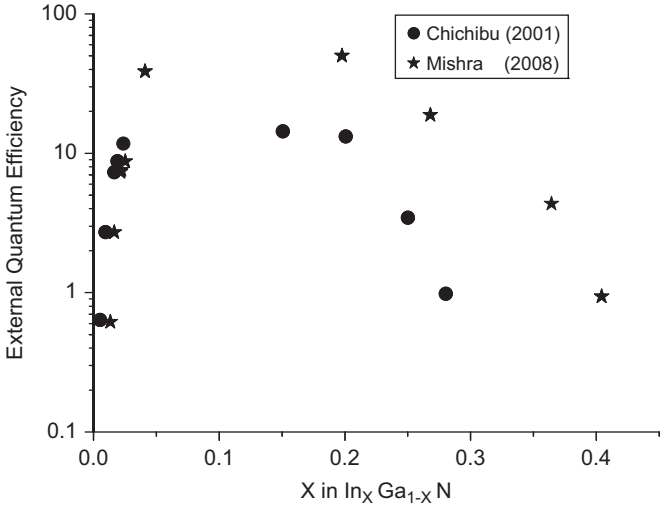

Fig. 7. External quantum efficiency of InGaN MQW LEDs versus x_{In} .The data points were obtained from Mishra [115] and Chichibu et al. [122].

evidence of localized (2D) recombination [8]. At the In concentrations used in blue and green LEDs, the effect appears to be due to PS, based on TEM data and the large Stokes shift. The doubts about InN-clustering have mainly been related to incorrect claims that spinodal decomposition cannot occur in InGaN layers and that TEM evidence of PS is unreliable. Both of these issues have been addressed in detail in Sections 2 and 3.

A major effect that may be related to the reduced radiative recombination in QW LED structures with high In content is the QCSE. Wurtzite AlGaInN alloys are piezoelectric. Thus, stress along the *c*-axis of InGaN in QWs will give rise to a piezoelectric field which decreases the overlap between electron and hole wavefunctions. This results in a decrease in the quantum efficiency for the production of visible photons. As the In concentration increases this QCSE increases. Thus, the efficiency of green LEDs would be expected to be lower than for blue LEDs. This is consistent with the well-known "green gap" observed experimentally. At the higher In concentrations required for yellow and red LEDs, the effect is even larger because of the increased piezoelectric field. This may, in part, explain their very low efficiencies. A beneficial effect of the QDs formed by PS may be that the deleterious effect of the QCSE is reduced by the formation of very small QDs, 1–2 nm in size. Of course, the wave function overlap will increase as the size of the QD decreases, because the electrons and holes are squeezed together. This presents a promising approach for the development of longer wavelength InGaN LEDs. Moustakis and co-workers used MBE to produce small QDs that were used for green LEDs [6,32]. This mechanism may also explain the improved yellow emission intensity obtained by Lai et al. [68] for InGaN grown by OMVPE which is found to spinodally decompose to produce small-sized clusters behaving as quasi-quantum dots. Park et al. [116] used the S–K process for the self-assembly of InGaN QDs to produce a 5 layer LED structure. They specifically reported improved LED performance as the size of the quantum dots was decreased.

In addition to increasing the radiative recombination efficiency, the presence of In-rich clusters due to PS in InGaN quantum wells has been the basis of explaining the recombination dynamics observed using time resolved spectroscopy. The results of Lu et al. [117] for 2.5 nm quantum wells with an In content of the well layer of 20%, compared samples having both high and low densities of the In-rich clusters due to spinodal decomposition. The differences were interpreted in terms of exciton trapping by the local potential minima due to the compositional inhomogeneities. Similar results were reported by Viswanath et al. [118]. They interpreted the large PL linewidth to inhomogeneous broadening from compositional fluctuations due to spinodal decomposition. The radiative and non-radiative lifetimes were deduced from the temperature dependence of the PL intensities and lifetimes and the results were interpreted in terms of the localization of excitons due to the inhomogenous In distribution.

Recently, several strategies have been developed for the use of PS in InGaN for the production of white LEDs. The basic idea is to generate yellow photons in the InN-rich regions and blue photons in the matrix. Together, the light produced will appear as white. This is a very promising approach for white LEDs because the other two techniques use either a blue LED and an overlayer of phosphor to down-convert some blue photons to yellow or the use of 3 (red, green, and blue) or sometimes 4 (adding yellow) individual LEDs packaged together. Both approaches have significant disadvantages. A white LED having only a single p/n junction and no phosphor is very attractive.

Several approaches have been used to foster and control PS in the InGaN for white LEDs. Park et al. [67] used roughening of the surface to facilitate PS. As described above, the surface roughening is believed to produce incoherent In-rich InGaN islands. Other groups have used the control of strain in the epitaxial layers, using partially or completely relaxed buried layers, to control PS. Strain from the substrate is believed to reduce spinodal decomposition, as described in Sections 2 and 3. Reducing the mismatch strain will have two effects; it will increase In incorporation, due to the lattice pulling effect, and it will enhance PS by reducing the strain in the InGaN layer. These approaches are novel and promising. Wang et al. [119] used spinodal decomposition to form InN-rich QDs. The 220 nm thick underlying layer, containing 5% In, is relaxed, since the thickness is much greater than t_c. This is followed by a GaN layer and then the MQW structure. Four, 3 nm thick InGaN layers, containing 17% In form the well layers. Thus, the InGaN QW layers are partially relaxed, enhancing PS due to spinodal decomposition. The EL spectra reported by Wang et al. [119] are reproduced Fig. 8. The yellow emission from the In-rich QDs and the blue emission from the more Ga-rich matrix are clearly resolved. The combined emission at high current densities looks white; thus, they have produced a white, single junction LED having no phosphor. These authors also demonstrated the production of In-rich regions using TEM, employing sample preparation techniques producing no artifacts to interfere with the interpretation of their results. The results are reproduced in Fig. 9. InN-rich regions, identified as "dots" are clearly distinguished.

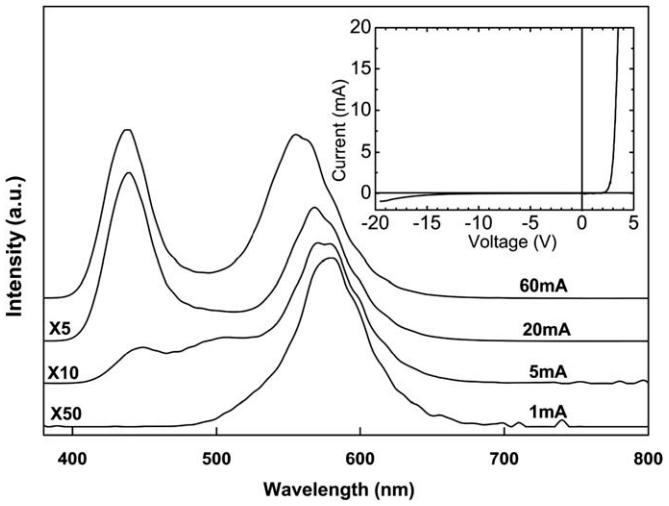

Fig. 8. Electroluminescence spectra of InGaN layers with In-rich clusters at several currents (after Wang [119]).

Lu et al. [120] also used an InGaN underlayer to reduce strain in the QW layers. They reported enhanced PS, as evidenced by TEM studies. Atomic level images using strain state analysis (SSA) yielded the In variation from QD to matrix in the light-emitting InGaN layers. They used changes in the thickness of the underlying, strain-relieving layer to produce values of the variation of In content from the In-rich region to the matrix of 14–18%, 15–25%, 17–37%, and 18–49% as the pre-strained layer thickness was decreased. For 5 period MQW structures with 3 nm InGaN well layers, the best results were obtained with a 5 nm thick underlying layer having 7% In. Obviously, this is less than the critical layer thickness, so the layers are coherent. Other researchers have used alternate techniques to induce PS. Soh et al. [121] also made white LEDs using In-rich quantum dots to produce the yellow emission. They used dual stacked MQWs, using a complex procedure that includes the use of In as an antisurfactant.

5. Summary

The materials phenomena that occur during the epitaxial growth of thin films of semiconductor alloys have been reviewed.

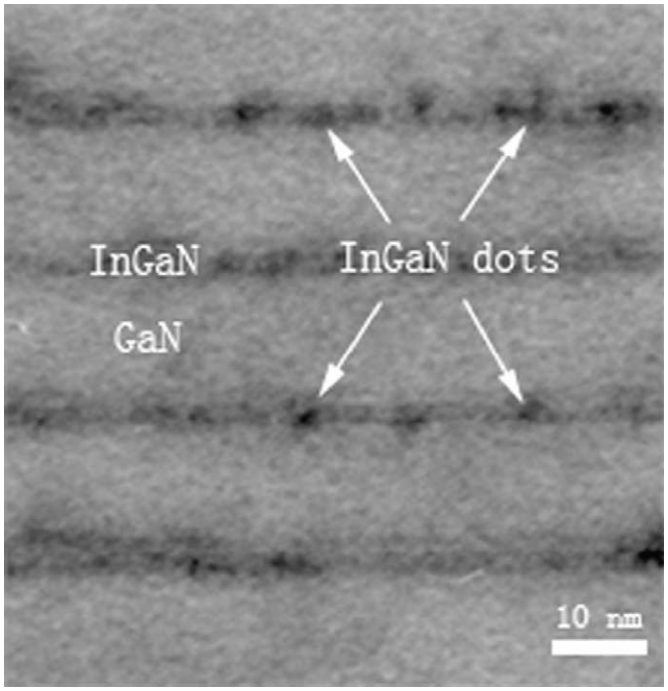

Fig. 9. Cross-section TEM image of the In-rich InGaN quantum dots in the LED structure giving the EL spectra shown in Fig. 8 (after Wang [119]).

They result in the formation of a variety of microstructures that are different in important ways from the ideal, random alloy. The focus of this paper has been on the formation of thin InGaN layers with a microstructure consisting of more than a single phase. PS can occur due to both lattice pulling and spinodal decomposition in these coherent InGaN layers. The former is driven by the effect of strain on the thermodynamics of the solid and the latter by the enthalpy of mixing of the alloy. In order to understand the microstructures formed it is vital to consider the thermodynamics of the structures in terms of the S–K growth mechanism, since the nano-scale islands formed allow the relaxation of strain without the introduction of misfit dislocations. For example, strain will suppress spinodal decomposition in a uniform film, but near the apex of a pyramidal island, the strain is relaxed so that PS may occur. The relaxation of strain also results in the accumulation of In near the top of the island due to lattice pulling. Thus, PS by two mechanisms may occur in the S–K islands formed spontaneously during coherent InGaN growth on a GaN underlayer.

The PS expected is indeed observed using a wide variety of techniques. The results for a number of X-ray, TEM, and optical techniques have been reviewed. They all indicate a non-random distribution of In in the InGaN epitaxial layers, including both thick, plastically relaxed layers and the coherent, ultra-thin layers used in QW structures for LED and laser devices. The formation of a high density of tiny, In-rich clusters is an intrinsic, thermodynamically-driven aspect of the epitaxial growth of thin, coherent InGaN layers. However, the morphology, as well as the size, extent of compositional fluctuation (Δx), and density will depend on the detailed growth conditions, as well as the composition and thickness of the layer.

The self-assembly of these microstructures by the S–K mechanism has a profound effect on the performance of devices, particularly blue, green, and white LEDs. The formation of these clusters increases the radiative recombination efficiency, the most important measure of device performance. This is due to the effects of quantum confinement in the tiny In-rich dots and due to the localization of recombination that prevents minority carriers from reaching the deleterious threading dislocations, formed with a high density during epitaxial growth. This occurs because the density of the In-rich QDs greatly exceeds the dislocation density. The spacing of the small bandgap regions that collect the minority carriers is experimentally observed to be from 2 to 10 nm, while the dislocation spacing is 100 nm, even for a dislocation density of 10^{10} cm^{-2}. Thus, the minority carriers injected into the active region at the p/n junction will traverse 10–50 low bandgap fluctuations, where they can be trapped, before reaching a dislocation. The controlled use of the QDs due to PS is a promising approach to the production of high-efficiency, inexpensive, single-junction, white LEDs. It also offers a promising approach to the eventual fabrication of high-efficiency yellow and red LEDs using the AlGaInN alloy system.

Acknowledgement

The author would like to thank Xiaobin Niu for help with preparing the figures.

References

[1] S. Nakamura, G. Fasol, in: The Blue Laser Diode: GaN Based Light Emitters and Lasers, Springer, Berlin, 1997.
[2] S. Nakamura in High Brightness LEDs, ed G.B. Stringfellow and M. G. Craford, Ch. 8; I. Akasaki and H. Amano, in High Brightness LEDs, ed G.B. Stringfellow and M. G. Craford, ch. 7.
[3] T.K. Ko, S.C. Shei, S.J. Chang, Y.Z. Chiou, R.M. Lin, W.S. Chen, S.F. Shen, C.S. Chang, K.W. Lin, IEEE. Proc. Optoelectron. 153 (2006) 212.
[4] Y. Okamoto, et al., IEEE. Trans. Electron Devices 51 (2004) 2217.
[5] O. Jani, I. Ferguson, C. Honsberg, S. Kurtz, Appl. Phys. Lett. 91 (2007) 132117.
[6] J. Abell, T.D. Moustakis, Appl. Phys. Lett. 92 (2008) 091901.
[7] T. Mukai, IEEE. J. Sel. Top. Quantum Electron. 8 (2002) 1077.
[8] For an excellent review, see N. Grandjean and M. Ilegems, Proceedings of IEEE 95 (2007) 1854.
[9] A.D. Lester, F.A. Ponce, M.G. Craford, D.A. Steigerwald, Appl. Phys. Lett. 66 (1995) 1249.
[10] E.F. Schubert, in: Light-Emitting Diodes, 2nd Edition, Cambridge, Cambridge, 2006.
[11] J. Wu, W. Walukiewicz, K.M. Yu, J.W. Ager, S.X. Li, E.E. Haller, H. Lu, W.J. Schaff, Solid State Commun. 127 (2003) 411.
[12] J. Wu, W. Walukiewicz, K.M. Yu, J.W. Ager, E.E. Haller, Hai Lu, W.J. Schaff, Phys. Status Solidi (b) 240 (2003) 412.
[13] G.B. Stringfellow, in: Organometallic Vapor Phase Epitaxy: Theory and Practice, 2nd Edition, Academic Press, Boston, 1999 Chapter 2.
[14] H.J. Kim, et al., J. Cryst. Growth 310 (2008) 3004.
[15] M. Allovon, J. Primot, Y. Gao, M. Quillec, J. Electron. Mater. 18 (1989) 505.
[16] M. Bosi, R. Fornari, J. Cryst. Growth 265 (2004) 434.
[17] C.P. Kuo, S.K. Vong, R.M. Cohen, G.B. Stringfellow, J. Appl. Phys. 57 (1985) 5428.
[18] G.B. Stringfellow, J. Appl. Phys. 43 (1972) 3455.
[19] see, for example; U. Nakajima, T. Ujihara, G. Sazaki, N. Usami, J. Cryst. Growth 220 (2000) 413;
M. del Rodriguez-Torrez, et al., J. Cryst. Growth 277 (2005) 138;
O.P. Chikalova-Luina, N.N. Ledentsov, E-J. Surf. Sci. Nanotech. 4 (2006) 53;
R.V. Wang, et al., Appl. Phys. Lett. 89 (2006) 221914;
A.A. Khandekar, J.Y. Yeh, L.J. Mawst, X. Song, S.E. Babcock, T.F. Kuech, J. Cryst. Growth 298 (2007) 154.
[20] F.C. Larche, J.W. Cahn, J. Appl. Phys. 62 (1987) 1232.
[21] Y. Kawaguchi, et al., J. Cryst. Growth 189-190 (1998) 24.
[22] S. Pereira, et al., Phys. Rev. B. 64 (2001) 205311;
M.R. Correia, et al., Appl. Phys. Lett. 85 (2004) 2235.
[23] H.Y. Lin, Y.F. Chen, T.Y. Lin, C.F. Shih, K.S. Liu, N.C. Chen, J. Cryst. Growth 290 (2006) 225.
[24] C.B. Soh, S.J. Chua, P. Chen, D.Z. Chi, W. Liu, H. Hartono, Thin Solid Films 515 (2007) 4509.
[25] M. Pristovsek, J. Stellmach, M. Leyer, M. Kneissl, Phys. Status Solidi C 6 (2009) 5565.
[26] G.B. Stringfellow, J. Cryst. Growth 27 (1974) 21.
[27] G.B. Stringfellow, M.G. Craford, in: High Brightness LEDs, Academic, Boston, 1997 Chapters 1–6.
[28] R.R. King, D.C. Law, K.M. Edmondson, C.M. Fetzer, G.S. Kinsey, H. Yoon, R.A. Sherif, N.H. Karam, Appl. Phys. Lett. 90 (2007) 183516.
[29] G.B. Stringfellow, in: A. Mascareneus (Ed.), Spontaneous Ordering in Semiconductor Alloys, Kluwer Academic/Plenum Press, New York, 2002 Chapter 3.
[30] G.B. Stringfellow, J.K. Shurtleff, R.T. Lee, C.M. Fetzer, S.W. Jun, J. Cryst. Growth 221 (2000) 1.

[31] L.C. Su, I.H. Ho, N. Kobayashi, G.B. Stringfellow, J. Cryst. Growth 145 (1994) 140.
[32] T.D. Moustakas, T. Xu, C. Thomidid, A.Y. Nikiforov, L. Zhou, D.J. Smith, Phys. Status Solidi (a) 205 (2008) 2560.
[33] I.H. Ho, G.B. Stringfellow, Appl. Phys. Lett. 69 (1996) 2701.
[34] E.L. Piner, N.A. El-Mastry, S.X. Liu, S.M. Bedair, Mater. Res. Soc. Proc. Vol. 482 (1998) 125;
N.A. El-Mastry, E.L. Piner, S.X. Liu, S.M. Bedair, Appl. Phys. Lett. 72 (1998) 40.
[35] F.A. Ponce, S. Srinivasan, A. Bell, L. Geng, R. Liu, M. Stevens, J. Cai, H. Omiya, H. Marui, S. Tanaka, Phys. Status Solidi (b) 2 (2003) 273.
[36] M. Rao, D. Kim, S. Mahajan, Appl. Phys. Lett. 85 (2004) 1961.
[37] D. Doppalapudi, S.N. Basu, K.F. Ludwig, T.D. Moustakas, J. Appl. Phys. 84 (1998) 1389;
R. Singh, D. Doppalapuki, T.D. Moustakas, L.T. Romano, Appl. Phys. Lett. 70 (1997) 1089.
[38] A. Kar, D. Alexson, M. Dutta, M.A. Stroscio, J. Appl. Phys. 104 (2008) 073502.
[39] N. Faleev, B. Jampana, O. Jani, H. Yu, R. Opila, I. Ferguson, C. Honsberg, Appl. Phys. Lett. 95 (2009) 051915.
[40] V. Potin, E. Hahn, A. Rosenauer, D. Gerthsen, B. Kuhn, F. Scholz, A. Dussaigne, B. Damilano, N. Grandjean, J. Cryst. Growth 262 (2004) 145.
[41] C.A. Tran, et al., J. Cryst. Growth 195 (1998) 397.
[42] F. Grosse, J. Neugebauer, Phys. Rev. B 63 (2001) 085207.
[43] S.Y. Karpov, N.I. Podolskaya, I.A. Zhmakin, A.I. Zhmakin, Phys. Rev. B 70 (2004) 235203.
[44] C.K. Gan, Y.P. Feng, D.J. Srolovitz, Phys. Rev. B 73 (2006) 235214.
[45] G.B. Stringfellow, J. Electron. Mater. 11 (1982) 903.
[46] S. Yu Karpov, MRS Internet J. Nitride Semicond. Res. 3 (1998) 16.
[47] T.L. McDevitt, S. Mahajan, D.E. Laughlin, W.A. Bonner, V.G. Keramidas, Phys. Rev. B 45 (1992) 6614.
[48] R.V. Kukta, L.B. Freund, J. Mech. Phys. Solids 45 (1997) 1835.
[49] J.A. Venables, in: Introduction to Surface and Thin Film Processes, Cambridge Press, Cambridge, 2000, p. 145–146.
[50] T.E. Vandervelde, R.M. Kalas, P. Kumar, T. Kobayashi, T.L. Pernell, J.C. Bean, J. Appl. Phys. 97 (2005) 043513.
[51] N.N. Ledentsov, D. Bimberg, Zh.I. Alferov, J. Lightwave Technol. 26 (2008) 1540.
[52] W. Siefert, N. Carlsson, J. Johansson, M. Pistol, L. Sammuelson, J Cryst. Growth 170 (1997) 39.
[53] see for example F.M. Ross, J. Tersoff, and R.M. Tromp, Phys. Rev. Lett. 80 (1998) 984 and references therein.
[54] D. Leonard, M. Krishnamurthy, C.M. Reaves, S.P. Denbaars, P.M. Petroff, Appl. Phys. Lett. 63 (1993) 3203.
[55] J.M. Moison, F. Houzay, F. Barthe, L. Leprince, E. Andre, O. Vatel, Appl. Phys. Lett. 64 (1994) 196.
[56] J.M. Gerard, O. Cabrol, B. Sermage, Appl. Phys. Lett. 68 (1996) 3123;
C. Weisbuch, J. Nagle, in: Science and Engineering of 1 D and 0 D Semiconductor Systems, ser. NATO ASI Series, Plenum, New York, 1990 p.319.
[57] K. Fu, Y. Fu, Appl. Phys. Lett. 94 (2009) 181913.
[58] T. Yamaguchi, S. Einfeldt, S. Gangodadhyay, A. Pretorius, A. Rosenauer, J. Falta, D. Hommel, Phys. Status Solidi (c) 3 (2006) 1396.
[59] W. Jung, J. Jang, S. Choi, J. Kim, Korean J. Mater. Res. 18 (2008) 535.
[60] K. Tachibana, T. Someya, A. Arakawa, Appl. Phys. Lett. 74 (1999) 383.
[61] N. Grandjean, J. Massies, Appl. Phys. Lett. 72 (1998) 1078.
[62] J.G. Lozano., A.M. Sanchez, R. Garcia, D. Gonzalez, O. Briot, S. Ruffenach, Appl. Phys. Lett. 88 (2006) 151913.
[63] W. Tasi, et al., Appl Phys. Lett. 94 (2009) 063102.
[64] D.I. Florescu, J.C. Ramer, V.N. Merai, A. Parekh, D. Lu, D.S. Lee, E.A. Armour, J. Cryst. Growth 272 (2004) 449.
[65] H. Hirayama, S. Tanaka, P. Ramvall, Y. Aoyagi, Appl. Phys. Lett. 72 (1998) 1736.
[66] C. Huang, T. Liu, Y. Lu, W. Shiao, Y. Chen, J. Wang, C. Lu, C.C. Yang, J. Appl. Phys. 104 (2008) 123106.
[67] I. Park, M. Kwon, S. Baek, Y. Ok, T.Y. Seong, S. Park, Y. Kim, Y. Moon, D. Kim, Appl. Phys. Lett. 87 (2005) 061906.
[68] Y. Lai, C. Liu, Z. Chen, Thin Solid Films 498 (2006) 128.
[69] N.V. Medhekar, V. Hegadekatte, V.B. Shenoy, Phys. Rev. Lett. 100 (2008) 106104.
[70] A. Lamaitre, G. Patriarche, F. Glas, Appl. Phys. Lett. 85 (2004) 3717.
[71] V. Perez-Solorzano, A. Groning, M. Jetter, T. Riemann, J. Christen, Appl. Phys. Lett. 87 (2005) 163121.
[72] Y. Tsai, R. Horng, M. Tseng, C. Kuo, P. Liu, D. Wuu, D. Lin, J. Cryst. Growth 311 (2009) 3220.
[73] M.R. Correia, S. Pereira, J. Frandon, I.M. Watson, C. Liu, E. Alves, A.D. Sequeira, N. Franco, Appl. Phys. Lett. 85 (2004) 2235.
[74] S.M. Pereira, M.R. Correia, E. Pereira, K.P. O'Donnell, C. Trager-Cowan, F. Sweeney, E. Alves, Phys. Rev. B 64 (2001) 205311.
[75] S.M. Pereira, K.P. O-Donnell, E.J. Alves, Adv. Funct. Mater. 17 (2007) 37.
[76] S. Pereira, Thin Solid Films 515 (2006) 164.
[77] P.R.C. Kent, A. Zunger, Appl. Phys. Lett. 79 (2001) 1977;
J.Z. Liu, A. Zunger, Phys. Rev. B 77 (2008) 205201.
[78] F. Glas, J. Appl. Phys. 62 (1987) 3210.
[79] J. Jalkanen, O. Trushin, E. Granato, S.C. Ying, T. Ala-Nissila, Eur. Phys. J. B 66 (2008) 175.
[80] N. Liu, J. Tersoff, O. Baklenov, A.L. Holmes, C.K. Shih, Phys. Rev. Lett. 84 (2000) 334.
[81] T. Yamaguchi, S. Einfeldt, S. Gangopadhyay, A. Pretorius, A. Rosenauer, J. Falta, D. Hommel, Phys. Status Solidi (c) 3 (2006) 1396.
[82] S.F. Chichibu, et al., Nat. Mater. 5 (2006) 817.
[83] S. Dalmasso, B. Damilano., N. Grandjean, J. Massies, M. Leroux, J.L. Reverchon, J.Y. Duboz, Thin Solid Films 380 (2000) 195.
[84] T. Kyono, H. Hirayama, K. Akita, T. Nakamura, K. Ishibashi, J. Appl. Phys. 98 (2005) 113514.
[85] T. Sugahara, M. Hao, T. Wang, D. Nakagawa, Y. Naoi, K. Nishino, S. Sakai, Jpn. J. Appl. Phys. Part 1 37 (1996) 2013.
[86] V. Kachkanov, K.P. O'Donnell, R.W. Martin, J.F.W. Mosselmans, S. Pereira, Appl. Phys. Lett. 89 (2006) 101908.
[87] T. Miyanaga, T. Azuhata, s Matsuda, Y. Ishikawa, S. Sasaki, T. Uruga, H. Tanida, S.F. Chichibu, T. Sota, Phys. Rev. B 76 (2007) 035314.
[88] K.P. O'Donnell, R.W. Martin, P.G. Middleton, Phys. Rev. Lett. 71 (1999) 237.
[89] V. Lemos, et al., Phys. Rev. Lett. 84 (2000) 3666.
[90] S. Chichibu, T. Azuhata, T. Sota, S. Nakamura, Appl. Phys. Lett. 69 (1996) 4188.
[91] Y. Narukawa, Appl. Phys. Lett. 70 (1997) 981.
[92] T.M. Smeeton, M.J. Kappers, J.S. Barnard, M.E. Vickers, C.J. Humphreys, Phys. Status Solidi A 240 (2003) 297.
[93] T.P. Bartel, P. Specht, J.C. Ho, C. Kisielowski, Phil. Mag. 87 (2007) 1983.
[94] T. Bartel, J.R. Jinschek, B. Freitag, P. Specht, C. Kisielowski, Phys. Status Solidi (a) 203 (2006) 167.
[95] J.R. Jimschek, R. Erni, N.F. Gardner, A.Y. Kim, C. Kisielowski, Solid State Commun. 137 (2006) 230.
[96] C. Kisielowski, T.P. Bartel, P. Specht, F.R. Chen, T.V. Shubina, Physica B 401-402 (2007) 639.
[97] T. Bartel, J.R. Jinschek, B. Freitag, P. Specht, C. Kisielowski, Phys. Status Solidi 203 (2006) 167.
[98] K. Okamoto, A. Kaneta, Y. Kawakami, S. Fujita, J. Choi, M. Terazima, T. Mukai, J. Appl. Phys. 98 (2005) 064503 see.
[99] S.F. Chichibu, K. Wada, J. Mullhauser, O. Brandt, K.H. Ploog, Appl. Phys. Lett. 76 (2000) 1671.
[100] S.F. Chichibu, et al., Phys. Status Solidi (a) 183 (2001) 91.
[101] A. Bell, J. Christen, F. Bertram, F.A. Ponce, H. Marui, S. Tanaka, Appl. Phys. Lett. 84 (2004) 58.
[102] T. Sugahara, M. Hao, T. Wang, D. Nakagawa, Y. Naoi, K. Nishino, S. Sakai, Jpn. J. Appl. Phys. 37 (Part 2) (1998) L1195.
[103] H. Sato, T. Sugahara, Y. Naoi, S. Sakai, Jpn. J. Appl. Phys. 37 (Part 1) (1998) 2013.
[104] S. Srinivasan, F. Bertram, A. Bell, F.A. Ponce, S. Tanaka, H. Omiya, Y. Nakagawa, Appl. Phys. Lett. 80 (2002) 550.
[105] S. Chichibu, T. Azuhata, T. Sota, S. Nakamura, Appl. Phys. Lett. 70 (1997) 2822.
[106] S. Chichibu, T. Azuhata, T. Sota, Appl. Phys. Lett. 79 (2001) 341.
[107] E.F. Schubert, I.D. Goepfert, W. Grieshaber, J.M. Redwing, Appl. Phys. Lett. 71 (2007) 921.
[108] R.W. Martin, P.G. Middleton, K.P. O'Donnell, W. Van der Stricht, Appl. Phys. Lett. 74 (1999) 263.
[109] Y. Narukawa, Y. Kawakami, S. Fujita, S. Fujita, S. Nakamura, PRB 55 (1997) R 1938.
[110] C. Kisielowski, Z. Liliental-Weber, S. Nakamura, Jpn. J. Appl. Phys. 36 (1997) 6932.
[111] P.G. Eliseev, P. Perlin, J. Lee, M. Osinki, Appl. Phys. Lett. 71 (1997) 596.
[112] T. Mukai, M. Yamada, S. Nakamura, Jpn. J. Appl. Phys. 37 (1998) 1358.
[113] Y. Narukawa, J. Narita, T. Sakamoto, K. Deguchi, T. Yamada, T. Mukai, Jpn. J. Appl. Phys. 45 (2006) L1084.
[114] S.F. Chichibu, T. Azuhata, M. Sugiyama, T. Kitamura, Y. Ishida, H. Okumura, H. Nakanishi, T. Sota, T. Mukai, J. Vac. Sci. Technol. B Volume 19 (2001) 2177.
[115] U. Mishra, "Group III nitride optoelectronics", Invited Talk, Electronic Materials Conference, Santa Barbara, Ca (2008).
[116] I. Park, M. Kwon, C. Cho, J. Kim, C. Cho, S. Park, Appl. Phys. Lett. 92 (2008) 253105.
[117] Y. Lu, C. Chen, H. Wang, C.C. Yang, J. Appl. Phys. 101 (2007) 063517.
[118] A.K. Viswanath, J.I. Lee, S.T. Kim, M. Yang, H.J. Lee, D. Kim, Thin Solid Films 515 (2007) 4401.
[119] X.H. Wang, H.Q. Jia, L.W. Guo, Z.G. Xing, Y. Wang, X.J. Pei, J.M. Zhou, H. Chen, Appl. Phys. Lett. 91 (2007) 161912.
[120] C. Lu, C. Huang, Y. Chen, C.C. Yang, J. Appl. Phys. 104 (2008) 043108.
[121] C.B. Soh, W. Liu, J.H. Teng, S.Y. Chow., S.S. Ang, S.J. Chua, Appl. Phys. Lett. 92 (2008) 261909.
[122] S.F. Chichibu, T. Azuhata, M. Sugiyama, T. Kitamura, Y. Ishida, H. Okumura, H. Nakanishi, T. Sota, T. Mukai, J. Vac. Sci. Technol. B 19 (2001) 2177.